分类号________ 密级__公开______

UDC __________ 编号_____________

江蘇大學

Master Thesis Dissertation

（硕 士 学 位 论 文）

The interaction between piles and layered transversely isotropic saturated soil

（桩基础和层状横观各向同性饱和土的相互作用）

指 导 教 师 Professor Lu Jian-Fei 作 者 姓 名 Uwiduhaye Fabrice

申请学位级别 Masters in Civil Engineering 专业名称 Structural Engineering

论文提交日期 2018.07 论文答辩日期 2018.09.14

学位授予单位和日期 江苏大学 2018.09

答辩委员会主席

评 阅 人__________

2018 年 9 月

独创性声明

本人郑重声明：所呈交的学位论文，是本人在导师的指导下，独立进行研究工作所取得的成果。除文中已注明引用的内容以外，本论文不包含任何其他个人或集体已经发表或撰写过的作品成果，也不包含为获得江苏大学或其他教育机构的学位或证书而使用过的材料 。对本文的研究做出重要贡献的个人和集体，均已在文中以明确方式标明。本人完全意识到本声明的法律结果由本人承担。

学位论文作者签名

2018 年 月 日

学位论文版权使用授权书

江苏大学、中国科学技术信息研究所、国家图书馆、中国学术期刊（光盘版）电子杂志社有权保留本人所送交学位论文的复印件和电子文档，可以采用影印、缩印或其他复制手段保存论文。本人电子文档的内容和纸质论文的内容相一致，允许论文被查阅和借阅，同时授权中国科学技术信息研究所将本论文编入《中国学位论文全文数据库》并向社会提供查询，授权中国学术期刊（光盘版）电子杂志社将本论文编入《中国优秀博硕士学位论文全文数据库》并向社会提供查询。论文的公布（包括刊登）授权江苏大学研究生处办理。

本学位论文属于不保密 □ 。

学位论文作者签名：　　　　　　　　　　指导教师签名：

2018 年　月　　　　　　　　　　2018 年　月

The interaction between piles and layered transversely isotropic saturated soil

桩基础和层状横观各向同性饱和土的相互作用

Major Structural Engineering

Supervisor Professor Lu Jian-Fei

Student name Uwiduhaye Fabrice

2018 年 7 月

The interaction between piles and layered transversely isotropic saturated soil

Abstract

In civil engineering, pile foundations are essential elements in structural design in soft soils. The fact that piles are driven deep into the ground thus to interact mostly with saturated soil layers, their interaction with surrounding soils remain one of the most urgently important parts of the whole structure. In this paper, the integral equation method is employed to develop a model that predicts the time-dependent behavior of an axially loaded pile embedded in a layered transversely isotropic saturated soil (TISS). Based on the fictitious pile method, the pile-soil system is decomposed into an extended saturated half-space and a fictitious pile. The extended half-space is treated as a layered TISS, while the fictitious pile is considered as a 1D bar. The fundamental solution of the layered TISS is gotten by the means of the RTM method for the layered TISS. The detailed contents of this paper consist of the following parts:

1. First, the RTM method is used to produce the elementary solutions, which corresponds to the time-dependent response of the layered TISS to a uniformly-distributed load acting vertically over a circular area with the radius equal to that of the pile. A system of partial differential equations is derived based on the governing equations of Biot's consolidation of TISS in cylindrical coordinate system. Then, employing the Hankel transforms and the Laplace transforms with respect to the radial coordinate r and the time t, respectively, a system of ordinary differential equations is derived in the transformed domain. Solving the differential equations will result in the general solution and the transform matrix relating the state vector

and the static wave vector is introduced. Later, the solution in the transformed domain to the layered TISS subjected to an external vertical force is deduced from the reflection and transmission matrices (RTMs) developed based on the wave vector transform matrix. The time domain solution to the layered TISS subjected to an external vertical force is retrieved with the use of the inverse Hankel-Laplace transform.

2. By using the fundamental solution developed for a layered TISS together with adopting the fictitious pile method due to Muki & Sternberg, the behavior of piles embedded in layered TISS is also studied in this paper. The pile-soil compatibility is accomplished by requiring that the axial strain of the fictitious pile be equal to the vertical strain of the extended layered TISS along the axis of the pile. The second kind Fredholm integral equation of the pile is then derived by using the aforementioned compatibility condition and the fundamental solution of the layered TISS. Applying the Laplace transform to the Fredholm integral equation, and solving the resulting integral equation, the transformed solution is obtained. Then the approximate time domain Fredholm integral equation of the second kind is obtained by the Schapery method.
3. Finally, employing the Fortran software, numerical results are obtained and discussed. First, an example is presented to discuss the impact of different soil parameters on the response of the layered TISS. Then, results obtained by the proposed integral equations for the pile agree with existing solutions very well, validating the proposed pile-soil interaction model. Later, using different

parametric examples, a parametric study is performed to examine the influence of some parameters of the pile-soil system on its response.

Keywords: pile; layered transversely isotropic saturated soil (TISS); consolidation; Fredholm integral equation; fictitious pile method.

桩基础和层状横观各向同性饱和土的相互作用

摘要

在土木工程中，桩基础是软土结构设计中的基本要素。由于桩被深深地推入地面，从而主要与饱和土层相互作用，它们与周围土壤的相互影响仍然是整个结构中最紧迫的重要部分之一。在本文中，采用积分方程方法开发了一个模型，该模型预测了嵌入层状横观各向同性饱和土（TISS）中的轴向荷载桩的时间依赖性。基于虚拟桩法，桩土系统分解为扩展的饱和半空间和虚拟桩。扩展的半空间被视为分层的TISS，而虚拟的堆被认为是一维条。分层 TISS 的基本解决方案是通过 RTM 方法获得的分层 TISS。本文的详细内容包括以下部分：

1. 首先，RTM 方法用于产生基本解，其对应于分层 TISS 对在圆形区域上垂直作用的均匀分布载荷的时间依赖性响应，该圆形区域的半径等于桩的半径。基于 Biot 在圆柱坐标系下固结 TISS 的控制方程，导出了偏微分方程组。然后，分别对径向坐标和时间采用 Hankel 变换和拉普拉斯变换，在变换域中导出常微分方程组。求解微分方程将导致一般解，并且引入与状态向量和静态波向量相关的变换矩阵。之后，从基于波矢量变换矩阵开发的反射和透射矩阵（RTM）推导出变换域中的受到外部垂直力的分层 TISS 的解。利用逆 Hankel-Laplace 变换检索受到外部垂直力的分层 TISS 的时域解。
2. 通过使用由分层 TISS 开发的基本解决方案以及采用 Muki＆Sternberg 的虚拟桩方法，本文还研究了嵌入在分层 TISS 中的桩的行为。通过要求虚拟桩的

轴向应变等于沿着桩轴的延伸分层 TISS 的垂直应变来实现桩 - 土相容性。然后通过使用上述兼容性条件和分层 TISS 的基本解来导出第二类 Fredholm 积分方程。将拉普拉斯变换应用于 Fredholm 积分方程，并求解得到的积分方程，得到变换后的解。然后通过 Schapery 方法得到第二类近似时域 Fredholm 积分方程。

3. 最后，使用 Fortran 软件，获得并讨论了数值结果。首先，提出一个例子来讨论不同土壤参数对分层 TISS 响应的影响。然后，通过所提出的堆积分方程得到的结果与现有解非常吻合，验证了所提出的桩 - 土相互作用模型。之后，使用不同的参数示例，进行参数研究以检查桩 - 土系统的一些参数对其响应的影响。

关键词： 桩;层状各向同性饱和土（TISS）;沉降; Fredholm 积分方程;虚拟桩法。

Contents

List of Tables

List of Figures

Notations

$-$: Superscript, Laplace transform

$\bullet$: Superscript, time derivative of a variable

(G) : Superscript, Fundamental solution

(v) : Order of the Hankel transform

ξ : Hankel transform parameter

s : Laplace transform parameter

$J_v(*)$: Bessel function of order v

r : Radial coordinate

θ : Angular coordinate

z : Vertical coordinate (axial)

z^* : Dimensionless depth

t : Time

t^* : Dimensionless time factor

R : Radius of circular load and pile

R^* : Dimensionless depth

d : Pile diameter

A : Pile cross-sectional area

L : Pile Length

h : Soil layer thickness

L_R : Reference length

Q : Vertical downward load on pile top

Q^* : Dimensionless vertical applied force

σ : Total stress

s^* : Dimensionless fundamental solution for the soil vertical stress

σ' : Effective stress

p : Soil pore pressure

p^{*} : Dimensionless pile-side soil pore pressure

p^{**} : Dimensionless fundamental solution for the soil pore pressure

σ_{rr} : Radial stress

σ_{zz} : Vertical stress

τ_{zr} : shear stress

$f_z(*)$: Force at $\Pi(z)$

$N(*)$: Pile axial force

N^{*} : Dimensionless pile axial force

$N_{*}(*)$: Fictitious l pile axial force

$q_v(*)$: Vertical distributed load along the fictitious pile

q_z , q_r : Rate of the fluid flow in t vertical and horizontal directions

u_z : Vertical displacement

u^{*} : Dimensionless pile vertical displacement

v^{*} : Dimensionless fundamental solution for the soil vertical displacement

u_r : Horizontal displacement

w^{*} : Dimensionless fundamental solution for the soil horizontal displacement

ε_r , ε_z : Horizontal and vertical strain

k_v , k_h : Coefficient of soil permeability in vertical and horizontal directions

k_R : Reference coefficient of soil permeability

v_{hv} : Soil Poisson's ratio of the horizontal strain caused by horizontal stress

v_{vh} : Soil Poisson's ratio of the vertical strain caused by horizontal stress

v_h : Soil Poisson's ratio in horizontal direction

E_h : Soil vertical Young's modulus

E_v : Soil Horizontal Young's modulus

E_p : Pile Young's modulus

E_{p^*} : Virtual pile Young's modulus

μ_v : Soil shear modulus

μ_R : Reference shear modulus

η : Soil stiffness ratio

m : μ_v / E_v

γ_w : Unit weight of water

ψ : State vector

u : displacement vector in state vector

f : stress vector in state vector

A : Coefficient matrix

λ_i, v_i : ith Eigenvalue and Eigenvector, respectively

M : Transform matrix relating the state vector to the static wave vector

w : Static wave vector

w_d, w_u : Down-going and Up-going wave vector

$T^{(w)}$: Wave vector transfer matrix

$T^{(s)}$: State vector transfer matrix

T_d, T_u : Transmission matrices for the down-going and up-going wave vectors

R_d, R_u : Reflection matrices for the down-going and up-going wave vectors

$\Pi(z)$: Circular area equivalent to the cross-section area of the pile with the vertical coordinate equal to z

Chapter 1 Introduction and literature review

1.1 Background

In civil engineering, pile foundations are essential elements in structural design in soft soils. They permit structures to be constructed upon weak or erratic soils by transferring loads of the building to a hard deeper soil layer. Piles vary in length, diameter, and material, which are all determined based on the given site conditions and loading. They can withstand axial loads, lateral loads or a combination of both, as long as they are designed in a proper way. These are required in special situations such as: where the upper soil layers are highly compressible and comparatively weak to support the whole load of the structure; the structure is subjected to horizontal forces; there is a presence of expansive soil; the foundation is subjected to uplifting forces; there is a possibility of the soil erosion at the surface of the ground due to water flows; etc. The fact that piles are driven deep into the ground thus to interact mostly with saturated soil layers, their interaction with surrounding soils remain one of the most urgently important parts of the whole structure.

Real saturated soils encountered in civil engineering are usually stratified and the properties of deferent layers may thus be different. Further, although most saturated soils are isotropic in the horizontal plane, due to the deposition process, moduli and permeability of the soil in the vertical direction are usually different from those in the lateral direction considerably (Figure 1.1). Thus, it makes more sense to treat the soil as a transversely isotropic saturated medium. As piles are the most widely used foundation type in the world, it is thus important to investigate the interaction between the piles and the layered transversely isotropic saturated soil (TISS).

So far a number of methods have been presented by different authors for the investigation of the pile-soil interaction. A few and important studies on the pile response in homogeneous and non-homogenous soil are presented in the following subsections.

1.1.1 Pile in homogenous soil

In early studies, several investigators [1-5] outlined approximate methods based on elastic theory for analyzing different aspects of the load-displacement behavior of single axially loaded piles and piers. Poulos and Davis [6, 7] proposed accurate analyses to the problem of the axial loading of incompressible floating piles embedded in an ideal elastic homogenous half-space by employing a discretization procedure. The interface between the bar and the elastic soil was discretized into a series of ring elements of finite length. The expressions for the axial displacement due to stresses acting vertically on these elements were derived by utilizing Mindlin's solution [8] for concentrated axial load acting at the interior of the half-space. Later, Mattes and Poulos [9] utilized a mirror image technique for end-bearing piles seated on a firm base. In order to eliminate the assumption of a smooth disc pile base and taking into consideration the disturbance of the half-space due to the presence of the piles that was ignored in the above mentioned studies, Butterfield and Banerjee [10] presented a rigorous analysis based on the Mindlin’s equations [8] together with the analytical method to study the response of a rigid and compressible single piles and pile groups with a floating cap in a homogeneous linear elastic soil. The effect of smooth disc pile base on under reamed piles and very short plain piles was shown to be significant, besides, the pile compressibility was also illustrated to be an important aspect in a pile group behavior.

Muki and Sternberg [11, 12] proposed an important approach for partially embedded rod in an elastic half-space under axial load based on an assumption that decomposes the bar-half-space system into a one-dimensional bar and an extended half-space. Such an assumption essentially reduces the problem to the solution of a Fredholm integral equation of the second kind in which the axial force in the rod becomes the primary unknown. Owing to the importance of this class of problems, various authors [13-17] have attempted to reformulate the problem within similar frameworks. For instance, on the basis of an energy principle and the Muki and Sternberg approach [11, 12], Rajapakse and Shah [18] proposed an approximate treatment of this problem through a discretization of the rod-medium interfacial tractions. Pak and Saphores [19] reconsidered the same problem by using Muki and Sternberg concepts, however, the displacement was taken as the basic unknown. To account for the influence of the pore pressure on the pile-soil interaction, Niumpradit & Karadushi [20] used the Biot's theory [21] of poroelasticity and the same fictitious pile method due to Muki & Sternberg to present the first time-dependent theoretical study which deals with the interaction between a pile and a saturated homogeneous half-space. However, only final and initial state solutions were obtained. Liang [22] analyzed the pile-to-pile interaction under different situations of consolidation for piles loaded vertically embedded in homogeneous poroelastic saturated half-space employing Muki and Sternberg approach.

1.1.2 Pile in non-homogenous soil

As mentioned earlier, piles are rarely embedded in an ideal homogenous single soil layer. Thus, to account for the soil non-homogeneity, Banerjee and Davies [23] employed the analytical solutions proposed by Davies and Banerjee [24] for a two-layered soil and analyzed the behavior axially and laterally loaded single piles embedded in a soil layer whose modulus increases linearly with depth. Randolph and Wroth [25] presented an approximate closed-form solution for the settlement of a pile in a Gibson soil [26], then, Guo and Randolph [27] extended this work with an elastic-plastic solution that considers the case of soil response with stiffness and strength varying as a power law of depth. Poulos [28] proposed an empirical technique, in which a modified soil modulus is used in the Mindlin solutions. Lee et al. [29] and Chin et al. [30] employed the fundamental solutions for an interior point load in a two-layered soil proposed by Chan et al. [31], then studied the response of axially loaded piles and pile groups in layered soils using a simple elastic continuum boundary element method, respectively. Chow [32] used the finite element method to present a numerical procedure that models axially loaded piles and pile groups embedded in non-homogeneous soil with transverse or cross-anisotropic behavior. Normally, the modulus of elasticity of adjacent layers of the soil may differ abruptly. Thus, the above solutions are only appropriate for axially loaded piles in a two-layered soil and they might not give accurate results for piles embedded in multilayered soil type.

1.1.3 Pile in multilayered soil

To account for the stratification of the realistic soil, a number of authors presented single phase solutions for single piles embedded in multilayered soils [33-37]. However, as mentioned before, in practical conditions piles do interact with saturated soils, thus time-dependent solutions will make more sense. Based on that, Senjuntichai et al. [38] studied the time-dependent response of an axially loaded bar in a multilayered poroelastic half-space by the influence function of the multilayered poroelastic half-space and the Laplace transform method. Modeling the pile with the finite element method and using the soil's fundamental solution obtained via the analytical layer-element method [39], Ai et al. [40] also provided a time-dependent solution for a pile embedded in a multilayered saturated soil. Most recently, by considering a soil medium with anisotropic permeability, Ai et al. [41] presented a solution for saturated multi-layered soils with overlying single-phase soils and analyzed the time-dependent response of pile embedded in layered saturated soils with elastic superstrata.

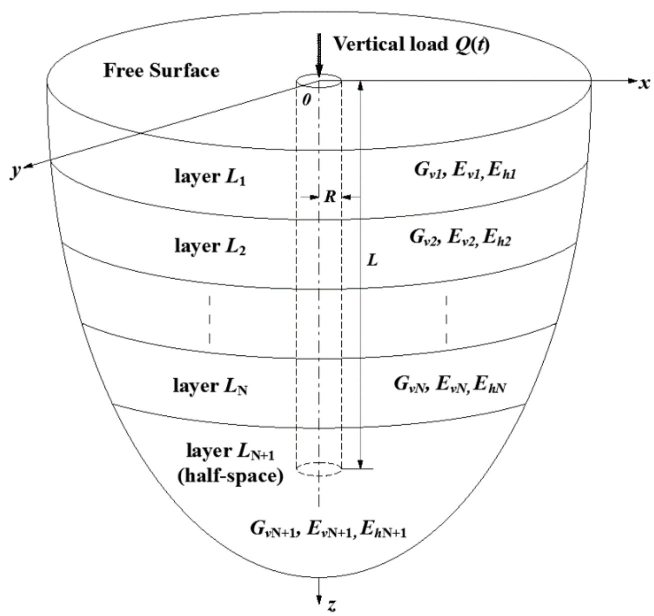

Figure 1. 1 Schematic of an axially loaded pile embedded in a layered TISS

As mentioned above, apart from stratification property, in engineering practice, the soil might exhibit transverse isotropy property [42-44]. However, researches about the time-dependent interaction between the vertically loaded pile and the Layered TISS have not been reported in the literature. Existing relevant researches are all concerned with the interaction between the pile and single phase transversely isotropic soil. For example, by treating the transverse isotropy property of the soil with a combination of the order reduction approach and the integral transform method, Ai & Yi [45] presented a boundary element method solution for a single pile embedded in a multilayered transversely isotropic soil. Later, Ai et al. [46] investigated the behavior of piles in a multilayered transversely isotropic soil subjected to vertical and horizontal loads simultaneously utilizing the fundamental solutions modeled via the Analytical layer element method [47].

To account for the above mentioned gap, this research utilizes the RTM method and the Integral equation method to analyze the interaction between single piles loaded vertically on top and the layered Transversely Isotropic Saturated Soil (TISS) at different times. It is noted that the soil and pile-soil interaction solutions presented in this paper will be time-dependent.

1.2 The main objective and research contents of this paper

The main objective of this paper is to develop a model that predicts the time-dependent behavior of a vertically loaded pile embedded in a layered TISS (Figure 1.1). To establish the model, the pile-soil structure is decomposed into an extended saturated half-space and a fictitious pile first, according to the fictitious pile method. The extended half-space is treated as a layered TISS, while the fictitious pile is as a 1D bar. The compatibility between the extended saturated half-space and the fictitious pile is accomplished by requiring that the vertical strain of the extended layered TISS along the axis of the pile is equal to the axial strain of the fictitious pile.

The specific structure and main contents of this thesis are as follows:

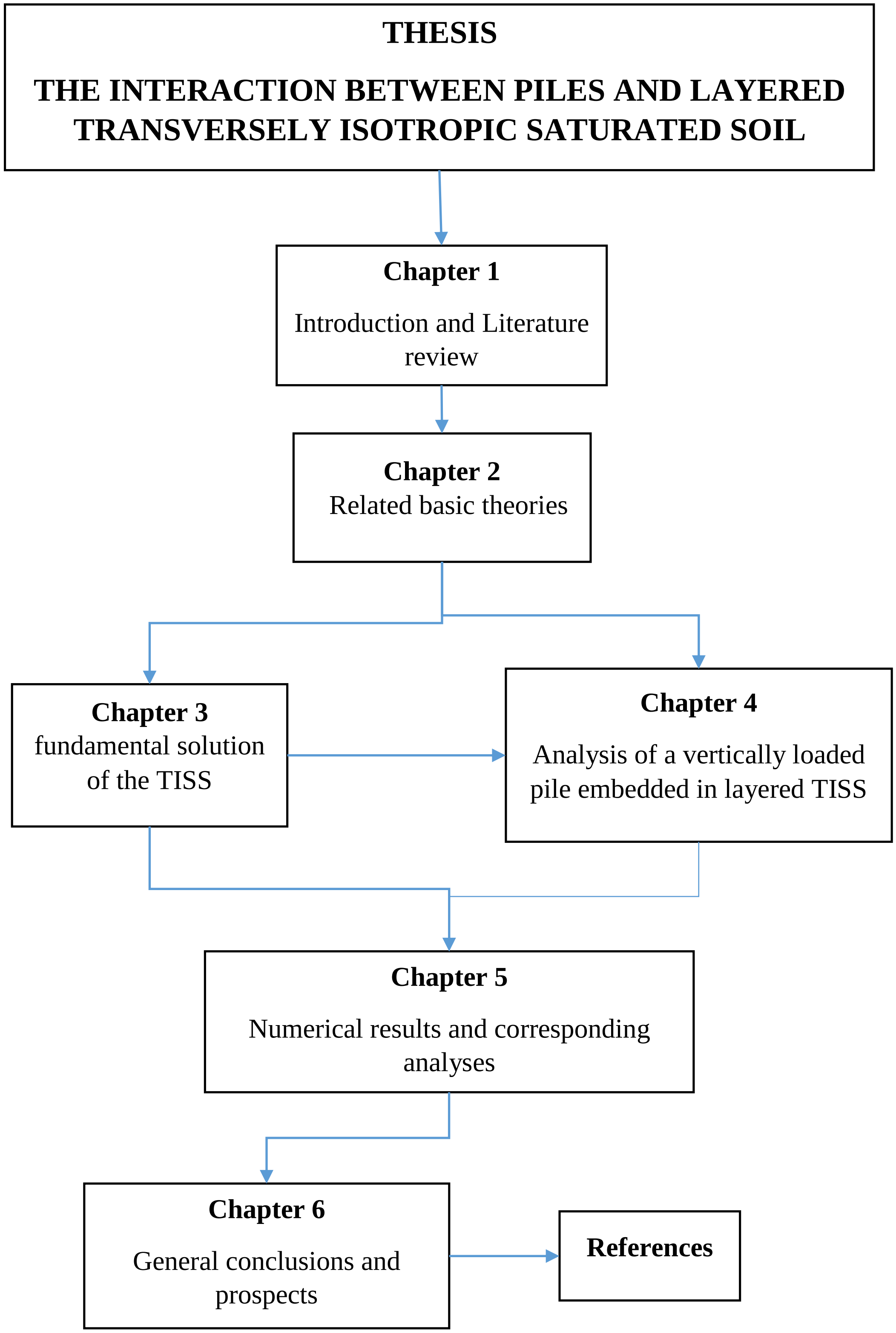

Figure 1. 2 Research technical route

Chapter 1 introduces the research background on the interaction between the piles and soil medium. This Chapter summarizes some of the most important methods and approaches adopted by different authors to investigate the behavior of loaded piles embedded in different types of mediums. The later vary from the ideal homogenous half-space to multilayered transversely isotropic soils. This provides the purpose and significance of the research and details the main objective of this paper.

Chapter 2 defines and details the basic mathematical transformation theories needed in later chapters, such as the Laplace transform and the Hankel transform and their respective inversions. This chapter also outlines the numerical solution method for the Fredholm integral equations of the second kind utilized later in **Chapter 4**.

Chapter 3 presents the fundamental solution of a layered Transversely Isotropic Saturated soil (TISS) subjected to a uniform distributed vertical load obtained via the reflection-transmission matrix (RTM) method originally developed for addressing the wave propagation problem in the layered elastic medium. The major variables used to develop the reflection and transmission matrices (RTMs) of the soil are obtained based on the governing equations of Biot's consolidation of TISS in the cylindrical coordinate system and the Hankel-Laplace transformations (**Chapter 2)**. Later, the solution in the transformed domain of the layered TISS subjected to an external vertical force is deduced from the reflection and transmission matrices (RTMs).

Based on the elementary solution obtained in **Chapter 3** together with adopting the fictitious pile method by Muki & Sternberg, **Chapter 4** details the formulation of the Fredholm integral equations of the second kind for the axially loaded pile embedded in the layered TISS. Chapters 4 also presents the progression of the numerical solution method for the second kind of Fredholm integral equations taking into account the layered soil type presented in this research.

With the aid of various graphs, **Chapter 5** discusses the numerical results obtained with the use of Fortran Program. First, the proposed model developed in this research is validated by comparing its numerical results to existing solutions. Then, different parametric examples are employed to examine the influence of some soil and pile parameters on the time-dependent behavior of the layered TISS subjected to a unit point force and the vertically loaded pile embedded in a layered TISS.

Finally, **Chapter 6** provides the general conclusion of the thesis and highlights some possible future prospects on piles interacting with layered TISS.

Chapter 2 Related basic theories

This chapter briefly introduces some of the basic mathematical theories used in later chapters of this paper. Namely, the Hankel transform, the Laplace transforms and the Fredholm integral equation.

2.1 Hankel Transform

Hankel transforms are integral transformations whose kernels are Bessel functions. Sometimes, they are referred to as Bessel transforms. In case problems that show axial symmetry are encountered (Chapter 3), Hankel transforms may be very useful.

2.1.1 Definition [48]

The νth order Hankel transform $\phi^{\nu}(\xi)$ of a function $\phi(r)$ defined for $r \geq 0$ is given by:

$$\phi^{(\nu)}(\xi) = \mathrm{H}_{\nu}\{\phi(r)\} = \int_0^{\infty} r\phi(r) J_{\nu}(\xi r) dr, \tag{2.1}$$

in which J_{ν} is the Bessel function of order ν and if $\nu \geq -1/2$, then, the Hankel's repeated integral immediately gives the following inversion formula:

$$\phi(r) = \mathrm{H}^{-1}{}_{\nu}\{\phi^{(\nu)}(\xi)\} = \int_0^{\infty} \xi \phi^{(\nu)}(\xi) J_{\nu}(\xi r) d\xi. \tag{2.2}$$

The two most important cases of the Hankel transform correspond to $\nu = 0$ and $\nu = 1$; these two cases will be used later in Chapter 3.

2.1.2 Hankel transform Properties

For any two arbitrary functions $\phi(r)$ and $\varphi(r)$, the Hankel transform have the following properties:

$$\mathrm{H}_v\{\phi(r)/r\} = \frac{\xi}{2v}(\mathrm{H}_{v-1}\{\phi(r)\} + \mathrm{H}_{v+1}\{\phi(r)\}), \tag{2.3}$$

$$\mathrm{H}_v\{\phi^{'}(r)\} = \frac{\xi}{2v}((m-1)\mathrm{H}_{v+1}\{\phi(r)\} - (m+1)\mathrm{H}_{v-1}\{\phi(r)\}), \tag{2.4}$$

$$\mathrm{H}_v\{\phi^{"}(r) + \phi^{'}(r)/r - \frac{v}{r^2}\phi(r)\} = -\xi^2\mathrm{H}_v\{\phi(r)\}, \tag{2.5}$$

$$\int_0^\infty \xi\mathrm{H}_v\{\phi(r)\}\mathrm{H}_v\{\varphi(r)\} = \int_0^\infty r\phi(r)\varphi(r)dr. \tag{2.6}$$

2.2 Laplace Transform

The Laplace transform is a powerful tool for treating many problems in mathematics, physics, and other applied and computational sciences. Primarily, this transform is very attractive in solving differential equations, since this takes a function of time and transforms it to a function of a complex variable s and because the transform is invertible, no information is lost. Therefore, it is reasonable to think of an arbitrary function $\phi(t)$ and its corresponding Laplace transform $\bar{\phi}(s)$ as two views of the same phenomenon.

2.2.1 Definition [48]

For a piecewise continuous function $\phi(t)$ on $[0,\infty)$, it is useful to define its Laplace transform, denoted by $L\{\phi(t)\} = \bar{\phi}(s)$ as a function of the complex variable $s = \sigma + j\omega$, where

$$\bar{\phi}(s) = \int_0^\infty \phi(t)e^{-st}dt. \tag{2.7}$$

The Laplace transform defined in the above equation (2.7) is sometimes called the one sided Laplace transform. However, There is a two sided version where the integral goes from $-\infty$ to ∞.

To recover the function $\phi(t)$ from its Laplace transform $\bar{\phi}(s)$, the inverse Laplace transform is introduced and can be defined by the following expression:

$$\phi(t) = L^{-1}\{\bar{\phi}(s)\} = \frac{1}{2\pi i}\int_{\alpha-i\infty}^{\alpha+i\infty} \bar{\phi}(s)e^{-st}dt \,, \tag{2.8}$$

where α is a parameter associated with the Laplace transform. Above equation (2.8) is correct if $\bar{\phi}$ is differentiable at the point t.

2.2.2 Properties of the Laplace transform

The following are some of the key properties of the Laplace transform used in this research:

Property 1. Linearity

$$L\{\alpha\phi_1(t) + \beta\phi_2(t)\} = \alpha L\{\phi_1(t)\} + \beta L\{\phi_2(t)\}. \tag{2.9}$$

Property 2. First Derivatives

$$L\{\phi^{'}(t)\} = sL\{\phi(t)\} - \phi(0). \tag{2.10}$$

Property 3. Second Derivatives

$$L\{\phi^{''}(t)\} = s^2L\{\phi(t)\} - s\phi(0) - \phi^{'}(0). \tag{2.11}$$

Property 4. Higher order derivatives

$$L\{\phi^{n}(t)\} = s^{n}L\{\phi(t)\} - s^{n-1}\phi(0) - s^{n-2}\phi^{'}(0) - \cdots - s\phi^{n-2}(0) - \phi^{n-1}(0). \tag{2.12}$$

Property 5. Convolution

Convolution in the time domain corresponds to multiplication in the frequency domain. Assume two arbitrary functions $\phi_1(t)$ and $\phi_2(t)$ with their corresponding Laplace transforms $L\{\phi_1(t)\} = \overline{\phi}_1(s)$ and $L\{\phi_2(t)\} = \overline{\phi}_2(s)$, respectively. Then, the convolution between $\phi_1(t)$ and $\phi_2(t)$ is defined by the following expression:

$$\phi_1(t) * \phi_2(t) = \int_0^t \phi_1(\tau)\phi_2(t-\tau)d\tau\ . \tag{2.13}$$

And the Laplace transform of the convolution between the two function $\phi_1(t)$ and $\phi_2(t)$ can be obtained as follows:

$$L\{\phi_1(t) * \phi_2(t)\} = \int_0^\infty \phi_1(t) * \phi_2(t) e^{-st} dt = \int_0^\infty \left[\int_0^t \phi_1(\tau)\phi_2(t-\tau)d\tau \right] e^{-st} dt\ . \tag{2.14}$$

The above equation (2.14) can also be written as

$$L\{\phi_1(t) * \phi_2(t)\} = \overline{\phi}_1(s)\overline{\phi}_2(s)\quad . \tag{2.15}$$

This implies that,

$$L^{-1}\{\overline{\phi}_1(s)\overline{\phi}_2(s)\} = \phi_1(t) * \phi_2(t)\ . \tag{2.16}$$

2.2.3 Numerical inversion of the Laplace transform

For simple cases, the inverse transform can be found via analytical methods or with the help of tables. However, it is not always easy to find the inverts. One possible reason is that the inverse is not a named function or cannot be represented by a simple formula. Due to the complexity of some expressions presented in this study, it is difficult to use analytical methods to retrieve solutions in the physical domain. Therefore, inversion of the Laplace transforms has to be carried out numerically. Fortunately, several numerical algorithms have been proposed in literature so far. These include Durbin's method [49], Stehfest's method [50] and Schapery's method [51]. Among the three methods, Schapery's method [51] is numerically more efficient for consolidation and rheological problems. Besides, its calculation is much more simple and time-saving. To account on this, inversion of the Laplace transforms in this study are carried out based on the Schapery's method [51].

2.3 Numerical solution for the Fredholm integral equations of the second kind

The general form of the Fredholm integral equation of the second kind is given by:

$$g(x) = f(x) + \lambda \int_a^b K(x,y) g(y) dy \, , \; a \le x, y \le b \, , \tag{2.17}$$

where $K(x,y)$ and $f(x)$ are the known functions and $g(x)$ the unknown function to be determined. Here, $K(x,y)$ is regarded as the kernel of the integral equation and λ as a (non-zero) regular value of the kernel.

Assume that $\int_a^b \phi(y) dy$ is approximated by the quadrature rule $J(\phi) = \sum_{j=0}^{n} \omega_j \phi(y_j)$. With such an approximation, for any $a \le x \le b$, the equation (2.17) can be reduced to:

$$\bar{g}(x) = f(x) + \lambda \sum_{j=0}^{n} \omega_j K(x, y_j) \bar{g}(y_j) \, , \tag{2.18}$$

where the solution $\bar{g}(x)$ will provide the approximation of the exact solution $g(x)$ in equation (2.17). A solution to the above equation (2.18) can be obtained with $x = y_i$, in which $i = 0,1,\ldots,n$ and $a \le y_i \le b$. Hence, equation (2.18) is therefore rewritten as:

$$\bar{g}(y_i) = f(y_i) + \lambda \sum_{j=0}^{n} \omega_j K(y_i, y_j) \bar{g}(y_j), \qquad i = 0,1,2,...,n. \tag{2.19}$$

Now, assume that $\bar{g}(y_0), \bar{g}(y_1), ...,$ and $\bar{g}(y_n)$ make a solution to equation (2.19). Thus, for any $x \in [a,b]$, equation (2.18) will have the following solution:

$$\bar{g}(x) = f(x) + \lambda \sum_{j=0}^{n} \omega_j K(x, y_j) \bar{g}(y_j) \,. \tag{2.20}$$

Supposing the second kind Fredholm integral equation of the following form:

$$Q(z) = a(z) f(z) + \int_0^L f(\xi) \frac{\partial \varepsilon(\xi, z)}{\partial \xi} d\xi \,, \quad 0 \le z \le L \,, \tag{2.21}$$

in which $Q(z), a(z)$ are known piecewise functions and $f(\xi)$ is the unknown function to be determined. Note that, in this research, similar second kind Fredholm integral equations will be encountered later in Chapter 4.

It is likely to use a numerical method in order to find a solution to the governing function $f(\xi)$ in the above Fredholm integral equation (2.21), due to the complexity of the kernel $\partial \varepsilon(\xi, z) / \partial \xi$, which can be shown to be discontinuous at $z = \xi$ (Chapter 3), thus an integrable logarithmic singularity at the same point $z = \xi$. Therefore, the integral in the above equation (2.21) can be reconstructed as follows

$$\int_0^L f(\xi) \frac{\partial \varepsilon(\xi, z)}{\partial \xi} d\xi = \int_0^{z^-} f(\xi) \frac{\partial \varepsilon(\xi, z)}{\partial \xi} d\xi + \int_{z^+}^{L} f(\xi) \frac{\partial \varepsilon(\xi, z)}{\partial \xi} d\xi \,. \tag{2.22}$$

With a numerical arrangement that separates the kernel into a singular and a continuous portion, Muki and Sternberg [12] solved an equation of this type, assuming $f(\xi)$ to be a continuous function and linear between two consecutive mesh-points of the interval. However, in this present study, a similar scheme can present problems, especially for a larger *L*.

In this study, the numerical technique used to solve the Fredholm integral equations of the pile was successfully used by Niumpradit & Karadushi [20] for an elastic pile in an ideal homogenous soil, in which the integration interval is divided into n segments and denoting each mesh point by $z_j, j = 1, 2, 3..., n+1$, in which $z_1 = 0$ and $z_{n+1} = L$. Then employing the trapezoidal integral formula on each segment, for every $z_j \le \xi \le z_{j+1}$, one has the following:

$$\int_{z_j}^{z_{j+1}} f(\xi) \frac{\partial \varepsilon(\xi, z)}{\partial \xi} d\xi = (1/2)[f(z_j) + f(z_{j+1})] \int_{z_j}^{z_{j+1}} \frac{\partial \varepsilon(\xi, z)}{\partial \xi} d\xi$$

$$= (1/2)[f(z_j) + f(z_{j+1})][\varepsilon(z_{j+1}, z) - \varepsilon(z_j, z)], \; z_j \le \xi \le z_{j+1}. \tag{2.23}$$

A similar method was also adopted by Lee and Rogers [52] in the solution of Volterra integral equations.

Thus, using the above equation (2.23), then the second kind Fredholm integral equation defined in equation (2.21) can be rewritten as:

$$Q(z_i) = a(z_i) f(z_i) + \sum_{j=1}^{n} (1/2)[f(z_j) + f(z_{j+1})][\varepsilon(z_{j+1}, z_i) - \varepsilon(z_j, z_i)],$$

$$i = 1, 2, ..., N+1. \tag{2.24}$$

With equation (2.24), a system of $n+1$ simultaneous equations, in which every value of $f(\xi)$ at z_j $(j=1,2,3...,n+1)$ can be obtained.

it is noted, however, due to the layered soil type presented in this research, new parameters such as N_L corresponding to the number of layers in contact with the pile will be later introduced and equation (2.24) will take a different form. More details are given in Chapter 4.

2.4 Summary

In this chapter, basic mathematical theories for transformation were reviewed. These include the Laplace transform and the Hankel transform together with their respective inversions. These transformation tools will be useful in solving differential equations later in **Chapter 3** and **Chapter 4.** Some of the basic terms and relations were derived for convenient uses later. At the end, this chapter also reviewed the definition of the Fredholm integral equations of the second kind, which is convenient in analyzing the pile-soil interaction. The numerical solution for the second kind Fredholm integral equations utilized in **Chapter 4** was also introduced and this will be more detailed later in the same **Chapter 4.**

Chapter 3 Fundamental solution for the layered Transversely Isotropic Saturated Soil (TISS)

In order to study the behavior of a vertically loaded pile embedded in a layered TISS, the fundamental solution reflecting the response of a layered saturated soil subjected to a uniform distributed load needs to be carried out in advance. In absence of the pile, the layered saturated soil will undergo an axisymmetric consolidation due to the same uniform distributed load, which acts over a circular domain and the radius is considered equal to that of the pile.

Based on Biot's theory of consolidation [21], a number of authors have addressed the consolidation problem of the layered saturated soil due to quasi-static loads with the use of different numerical and analytical methods. These include the finite layer method [53-55], the finite element method [56, 57], the boundary element method [58, 59] and the transfer matrix method [60, 61]. Furthermore, other analytical techniques have been developed to solve Biot's consolidation problems, such as Yue and Selvadurai [62], Pan [63].

To account on the sedimentation process and the variation of the orientation in different directions of the soil, resulting in different soil's Young's modulus in both horizontal and vertical direction as mentioned earlier, it is thus necessary to consider the property of transverse isotropy presented by most engineering soils. So far, the transfer matrix method [43, 44] seems to be one of the most efficient methods to solve consolidation problems in multilayered soils such as TISS due to the fact that it presents a good accuracy and convenient for computation. However, due to the presence of functions of exponential growth in the transfer matrices, this method presents an intrinsic fault that leads to illconditioned matrices for thick layer and this may raise some numerical instability for large thickness layers.

Originally, the reflection-transmission matrix (RTM) method [64, 65] was developed for addressing the wave propagation problem in the layered elastic medium and in the past few years, this method has been used to address problems of consolidation of layered saturated soils [66, 67] due to its ability to eliminate the positive exponential term for stable numerical algorithm. In this chapter, a similar method (RTM) is developed to investigate the consolidation behavior of a layered transversely isotropic saturated soil (TISS) subjected to a uniform distributed vertical load, which acts over a circular domain.

First, Based on the governing equations of Biot's consolidation of TISS in cylindrical coordinate system, a system of differential equations is derived in the transformed domain with the use of the Hankel transforms and the Laplace transforms with respect to the radial coordinate r and the time t, respectively. Solving the differential equations will result in the general solution and the transform matrix relating the state vector and the static wave vector is introduced. Later, the solution to the layered TISS subjected to an external vertical force is deduced from the reflection and transmission matrices (RTMs) developed based on the wave vector transform matrix. Note that the externally applied point load is prescribed either on the ground surface or within the soil layers.

3.1 Governing equations for the TISS

In this section, the governing equations of the layered TISS will be presented and these will help in the derivation of the general solution for the layered TISS. In the cylindrical coordinate system, the equilibrium equations for the TISS for the axisymmetric condition are as follows:

$$\frac{\partial\sigma_{rr}^{(G)}}{\partial r}+\frac{\partial\tau_{zr}^{(G)}}{\partial z}+\frac{\sigma_{rr}^{(G)}-\sigma_{\theta\theta}^{(G)}}{r}=0,\ \frac{\partial\sigma_{zz}^{(G)}}{\partial z}+\frac{\partial\tau_{zr}^{(G)}}{\partial r}+\frac{\tau_{zr}^{(G)}}{r}=0, \tag{3.1}$$

where $\sigma_{zz}^{(G)}$, $\sigma_{rr}^{(G)}$ and $\sigma_{\theta\theta}^{(G)}$ are the component of the total normal stress; $\tau_{zr}^{(G)}$ is the total shear stress component. For the saturated soil, the effective stress principle can be represented as follows:

$$\sigma^{(G)}=\sigma'^{(G)}+p^{(G)}, \tag{3.2}$$

in which $\sigma^{(G)}=\left\{\sigma_{rr}^{(G)},\sigma_{\theta\theta}^{(G)},\sigma_{zz}^{(G)},\tau_{zr}^{(G)}\right\}^T$; $\sigma'^{(G)}=\left\{\sigma'^{(G)}_{rr},\sigma'^{(G)}_{\theta\theta},\sigma'^{(G)}_{zz},\tau'^{(G)}_{zr}\right\}^T$; and $p^{(G)}=\left\{p^{(G)},p^{(G)},p^{(G)},0\right\}^T$ denote the total stress; the effective stress; and the pore pressure vectors, respectively. For the TISS, the constitutive relations for the effective stress have the following expressions:

$$\sigma'^{(G)}_{rr}=-\frac{\partial u_r^{(G)}}{\partial r}c_{11}-\frac{u_r^{(G)}}{r}c_{12}-\frac{\partial u_z^{(G)}}{\partial z}c_{13},\ \sigma'^{(G)}_{\theta\theta}=-\frac{\partial u_r^{(G)}}{\partial r}c_{12}-\frac{u_r^{(G)}}{r}c_{11}-\frac{u_z^{(G)}}{\partial z}c_{13},$$

$$\sigma'^{(G)}_{zz}=-\frac{\partial u_r^{(G)}}{\partial r}c_{13}-\frac{u_r^{(G)}}{r}c_{13}-\frac{\partial u_z^{(G)}}{\partial z}c_{33},\ \tau'^{(G)}_{zr}=-2\frac{1}{2}\left(\frac{\partial u_r^{(G)}}{\partial z}+\frac{\partial u_z^{(G)}}{\partial r}\right)c_{44}, \tag{3.3}$$

where $u_r^{(G)}$ and $u_z^{(G)}$ are the displacement components in *r* and *z* directions, respectively. The parameters $c_{11}\sim c_{44}$ denote the elastic constants of the TISS, which can be expressed as follows:

$$c_{11}=\frac{E_{\mathrm{h}}\left(1-\eta\nu_{\mathrm{hv}}^2\right)}{\left(1+\nu_{\mathrm{h}}\right)\left(1-\nu_{\mathrm{h}}-2\eta\nu_{\mathrm{hv}}^2\right)},\ c_{12}=\frac{E_{\mathrm{h}}\left(\nu_{\mathrm{h}}+\eta\nu_{\mathrm{hv}}^2\right)}{\left(1+\nu_{\mathrm{h}}\right)\left(1-\nu_{\mathrm{h}}-2\eta\nu_{\mathrm{hv}}^2\right)},$$

$$c_{13}=\frac{E_{\mathrm{h}}\nu_{\mathrm{hv}}}{1-\nu_{\mathrm{h}}-2\eta\nu_{\mathrm{hv}}^{2}},\ c_{33}=\frac{E_{\mathrm{v}}\left(1-\nu_{\mathrm{h}}\right)}{1-\nu_{\mathrm{h}}-2\eta\nu_{\mathrm{hv}}^{2}},\ c_{44}=\mu_{\mathrm{v}},\ \eta=\frac{E_{\mathrm{h}}}{E_{\mathrm{v}}}=\frac{\nu_{\mathrm{vh}}}{\nu_{\mathrm{hv}}}, \tag{3.4}$$

where E_{h}; E_{v}; and μ_v are the horizontal elastic modulus; the vertical elastic modulus and the vertical direction shear modulus of the soil, respectively. v_{h} is the Poisson's ratio of the soil in the horizontal direction; v_{hv} is the Poisson's ratio of the horizontal strain caused by the vertical stress; v_{vh} is the Poisson's ratio of vertical strain caused by horizontal stress and η denotes the ratio of the horizontal elastic modulus to the vertical elastic modulus of the soil.

In accordance with Darcy's law, the expression of the rate of the fluid flow in the z and r directions have the following form:

$$q_r^{(G)}=-k_h'\ \frac{\partial p^{(G)}}{\partial r},\ q_z^{(G)}=-k_v'\ \frac{\partial p^{(G)}}{\partial z},\ k_v'\ =k_v/\gamma_w,\ k_h'\ =k_h/\gamma_w, \tag{3.5}$$

in which k_v and k_h represent both the permeability of the soil in the vertical and horizontal directions, respectively. γ_w is the specific weight of water. By using equation (3.5), the seepage continuity condition for the TISS at time t can be written as:

$$\frac{\partial e}{\partial t}+k_h'\ \left(\frac{\partial^2}{\partial r^2}+\frac{1}{r}\frac{\partial}{\partial r}\right)p^{(G)}+k_v'\ \frac{\partial^2 p^{(G)}}{\partial z^2}=0,\ e=-(\frac{\partial u_r^{(G)}}{\partial r}+\frac{u_r^{(G)}}{r}+\frac{\partial u_z^{(G)}}{\partial z}), \tag{3.6}$$

in which e denotes the dilatation of the soil skeleton.

3.2 The general solution to the governing equations for the TISS

combining equations (3.2) and $(3.3)_4$, one has the following relation:

$$\frac{\partial u_r^{(G)}}{\partial z} = -\frac{\partial u_z^{(G)}}{\partial r} - \frac{\sigma_{zr}^{(G)}}{c_{44}}\,. \tag{3.7}$$

Similarly, using both equations (3.2) and $(3.3)_3$, the change of the displacement in z direction is obtained as:

$$\frac{\partial u_z^{(G)}}{\partial z} = -\frac{c_{13}}{c_{33}}\left(\frac{\partial u_r^{(G)}}{\partial r} + \frac{u_r^{(G)}}{r}\right) + \frac{\left(p^{(G)} - \sigma_{zz}^{(G)}\right)}{c_{33}}\,. \tag{3.8}$$

Then, using above equation (3.8) and both equation $(3.5)_2$ and (3.6), it yields:

$$\frac{\partial q_z^{(G)}}{\partial z} = \left(\frac{c_{13}}{c_{33}} - 1\right)\frac{\partial}{\partial t}\left(\frac{\partial u_r^{(G)}}{\partial r} + \frac{u_r^{(G)}}{r}\right) - \frac{1}{c_{33}}\frac{\partial}{\partial t}\left(p^{(G)} - \sigma_{zz}^{(G)}\right)$$

$$+k_h'\left(\frac{\partial^2}{\partial r^2} + \frac{1}{r}\frac{\partial}{\partial r}\right)p^{(G)}\,. \tag{3.9}$$

Rearranging both equation $(3.1)_2$ and $(3.5)_1$, turns into the following relations, respectively:

$$\frac{\partial \sigma_{zz}^{(G)}}{\partial z} = -\frac{\partial \tau_{zr}^{(G)}}{\partial r} - \frac{\tau_{zr}^{(G)}}{r}\,; \tag{3.10}$$

$$\frac{\partial p^{(G)}}{\partial z} = -\frac{1}{k_v'}q_z^{(G)}\,. \tag{3.11}$$

Finally, let's combine equations $(3.1)_1$, $(3.3)_{1,2}$ and (3.8) to obtain the following equation:

$$\frac{\partial \tau_{zr}^{(G)}}{\partial z} = \left(c_{11} - \frac{{c_{13}}^2}{c_{33}}\right)\left(\frac{\partial^2 u_r^{(G)}}{\partial r^2} + \frac{1}{r}\frac{\partial u_r^{(G)}}{\partial r} - \frac{u_r^{(G)}}{r^2}\right) + \frac{c_{13}}{c_{33}}\left(1 - \frac{\partial \sigma_{zz}^{(G)}}{\partial r}\right) - \frac{\partial p^{(G)}}{\partial r}\,. \tag{3.12}$$

At this stage, observing equations (3.7) to (3.12), it is worth defining the following six-dimensional state vector $\boldsymbol{\psi}(r,z,t)$ for a TISS undergoing axisymmetric consolidation as:

$$\frac{\partial \boldsymbol{\psi}(r,z,t)}{\partial z} = \mathbf{A}\left(r,t\right)\boldsymbol{\psi}(r,z,t),\ \boldsymbol{\psi}(r,z,t) = \left\{\mathbf{q}(r,\mathrm{z},t), \mathbf{f}(r,\mathrm{z},t)\right\}^T, \tag{3.13}$$

in which $\mathbf{q}(r,\mathrm{z},t) = \left\{u_z^{(G)}, u_r^{(G)}, q_z^{(G)}\right\}^T$ and $\mathbf{f}(r,\mathrm{z},t) = \left\{\sigma_{zz}^{(G)}, \tau_{zr}^{(G)}, p^{(G)}\right\}^T$ refer to the state vectors which denote the generalized displacement and stress vectors. The coefficient matrix $\mathbf{A}\left(r,t\right)$ defined in the above system of partial differential equations of the state vector defined in equation (3.13) can be found in the appendixes (I).

In order to derive the standard matrix differential equation, it is convenient to introduce the integral transformation methods (the Laplace and Hankel transform) defined earlier in Chapter 2 to remove the dependence upon the time t and radial coordinates r of the matrix $\mathbf{A}\left(r,t\right)$. Besides, these transformations will reduce the system of partial differential equations of consolidation mentioned above to the system of ordinary differential equations. Thus, referring to both equation (2.1) and (2.7), the following vth order Laplace–Hankel transform can be introduced:

$$\bar{\phi}^{(v)}(\xi,z,s) = \int_0^\infty \int_0^\infty e^{-st} r\phi(r,z,s) J_v(\xi r) dr dt\,, \tag{3.14}$$

in which ξ and s are the Hankel and Laplace transform parameters. $J_v(\xi r)$ denotes the vth order Bessel function and the superscript v represents the order of the Hankel transform.

It is noted that the superscript (G) notation denoting the fundamental solution parameters will be omitted throughout the remaining part of this chapter for better presentation of the Hankel transform superscript notation. However, this will again be used in the following Chapters.

Employing the above Hankel-Laplace transformation defined in equation (3.14) to the equations (3.7)-(3.12), these equations can finally be expressed in the form of a matrix ordinary differential equation, i.e.,

$$\frac{d\bar{\boldsymbol{\psi}}(\xi,z,s)}{dz} = \bar{\mathbf{A}}(\xi,s)\bar{\boldsymbol{\psi}}(\xi,z,s)\,, \tag{3.15}$$

where $\bar{\boldsymbol{\psi}}(\xi,z,s) = \left\{\bar{u}_z^{(0)}, \bar{u}_r^{(1)}, \bar{q}_z^{(0)}, \bar{\sigma}_{zz}^{(0)}, \bar{\tau}_{zr}^{(1)}, \bar{p}^{(0)}\right\}^T$ denotes the state vector in the transformed domain and the coefficient matrix

$$\bar{\mathbf{A}}(\xi,s) = \begin{bmatrix} \mathrm{A}_1 & \mathrm{A}_2 \\ \mathrm{A}_3 & \mathrm{A}_4 \end{bmatrix} \quad , \quad \mathrm{A}_1 = \begin{bmatrix} 0 & -a_2\xi & 0 \\ \xi & 0 & 0 \\ 0 & (a_2-1)s\xi & 0 \end{bmatrix} \quad , \quad \mathrm{A}_2 = \begin{bmatrix} -a_3 & 0 & a_3 \\ 0 & -a_1 & 0 \\ a_3 s & 0 & -a_3 s - k_h'\xi^2 \end{bmatrix} \quad ,$$

$$\mathrm{A}_3 = \begin{bmatrix} 0 & 0 & a_3 \\ 0 & -a_4\xi^2 & 0 \\ 0 & 0 & -1/k_v' \end{bmatrix}, \ \mathrm{A}_4 = \begin{bmatrix} 0 & -\xi & 0 \\ a_2\xi & 0 & (1-a_2)\xi \\ 0 & 0 & 0 \end{bmatrix}, \tag{3.16}$$

in which $a_1 = 1/c_{44}$, $a_2 = c_{13}/c_{33}$, $a_1 = 1/c_{33}$, and $a_4 = (c_{11}c_{33} - c_{13}^2)/c_{33}$.

Since the matrix differential equation given in equation (3.15) only depends on one variable z after employing the above mentioned integral transformations, then, the general solution to the state vector $\bar{\boldsymbol{\psi}}(\xi,z,s)$ in the transformed domain can be obtained easily. However, this demands a study on the Eigenvalues and their corresponding Eigenvectors of the matrix $\bar{\mathbf{A}}(\xi,s)$ denoted as λ and v, respectively. Thus, the characteristic equation of the matrix $\bar{\mathbf{A}}(\xi,s)$ can be obtained as follows:

$$\lambda^6 + b_2\lambda^4 + b_1\lambda^2 + b_0 = 0\,, \tag{3.17}$$

in which $b_0 = [-a_3 s\xi^4 - (a_2^2 + a_3a_4)k_h'\xi^6]/k_v'$, $b_2 = -[a_3 s + (k_h' - 2a_2k_v' + a_1a_4k_v')\xi^2]/k_v'$ and $b_1 = ([-2a_3 + a_1\{(a_2-1)^2 + a_3a_4\}]s\xi^2 + (-2a_2k_h' + a_1a_4k_h' + a_2^2k_v' + a_3a_4k_v')\xi^4)/k_v'$.

It is noted that the characteristic equation (3.17) of the matrix $\bar{\mathbf{A}}(\xi,s)$ can be obtained from the following equation:

$$\left[\bar{\mathbf{A}}(\xi,s) - \lambda \mathrm{I}_{6\times 6}\right]\mathrm{v}=0 \quad , \tag{3.18}$$

where $\mathrm{I}_{6\times 6}$ denotes the 6×6 identity matrix. The above equation (3.18) will have a non-zero solution v if and only if the determinant of the matrix $\left[\bar{\mathbf{A}}(\xi,s) - \lambda \mathrm{I}_{6\times 6}\right]$ is zero. Therefore, the Eigenvalues of $\bar{\mathbf{A}}(\xi,s)$ are values of λ that satisfy the equation $\left|\bar{\mathbf{A}}(\xi,s) - \lambda \mathrm{I}\right| = 0$.

In order to determine the six possible roots for the equation (3.17), it is worth assuming $\mathrm{y}=\lambda^2$ due to the fact that only even power terms appear in the equation. Thus, equation (3.17) yields the following cubic equation:

$$\mathrm{y}^3 + b_2\lambda^2 + b_1\lambda + b_0 = 0\,, \tag{3.19}$$

in which the Eigenvalues λ of the matrix $\bar{\mathbf{A}}(\xi,s)$ can be obtained as square roots of the roots of the equation (3.19), i.e., $\lambda=\pm\sqrt{\mathrm{y}}$. Therefore, the six possible Eigenvalues of the matrix $\bar{\mathbf{A}}(\xi,s)$ can be represented as follows:

$$\lambda_i = -\sqrt{\mathrm{y}_i} = -\gamma_i + \mathrm{i}\alpha_i\,,\ i = 1,2,3\,;$$

$$\lambda_j = +\sqrt{\mathrm{y}_i} = -\lambda_i\,,\ j = 4,5,6\,, \tag{3.20}$$

where $-\gamma_i$ and $\mathrm{i}\alpha_i$ is referred to as the real and imaginary part of the root, respectively. To be convenient, the parameter Δ is introduced as follows:

$$\Delta = \left(\frac{q_e}{2}\right)^2 + \left(\frac{p_e}{3}\right)^3, \tag{3.21}$$

with $p_e = b_1 - (b_2^{\ 2}/3)$ and $q_e = b_0 + (2b_2^{\ 3}/27) - (b_2 b_1/3)$.

As mentioned earlier, the general solution to the system of ordinary differential equations given in equation (3.15) depends on both the Eigenvalues and vectors of the transformed matrix $\bar{\mathbf{A}}(\xi,s)$ which have to be determined in advance. The latter can be obtained as the solution to equation (3.19). As for the solution to the cubic equation (3.19), three different Cases can occur depending on the sign of the parameter Δ introduced in equation (3.21). Namely, Case one ($\Delta > 0$), Case two ($\Delta < 0$), and Case three ($\Delta = 0$).

Case one

For a positive Δ, equation (3.19) has one real root y_1 and two complex conjugate roots, namely, $y_3 = y_2^\dagger$, where the symbol $\dagger$ denotes the conjugate. This implies that two of the six Eigenvalues of the matrix $\bar{\mathbf{A}}(\xi,s)$ are real, namely, λ_1 and λ_4, while other four, i.e., $\lambda_2, \lambda_3, \lambda_5$, and λ_6 are complex as shown below:

$$\lambda_1 = -\sqrt{y_1} = -\gamma_1\,,\ \lambda_2 = -\sqrt{y_2} = -(\gamma_2 + \mathrm{i}\alpha)\,,\ \lambda_3 = -\sqrt{y_3} = -\sqrt{y_2^\dagger} = -(\gamma_3 - \mathrm{i}\alpha)\,,$$

$$\lambda_4 = -\lambda_1 = \gamma_1\,,\ \lambda_5 = -\lambda_2 = \gamma_2 + \mathrm{i}\alpha\,,\ \lambda_6 = -\lambda_3 = \gamma_3 - \mathrm{i}\alpha\,, \tag{3.22}$$

in which $\gamma_3 = \gamma_2$, considering the relation $y_3 = y_2^{\dagger}$. In this case, since λ_1 and λ_4 are real, then, their corresponding Eigenvectors v_1 and v_4 are real. However, as $\lambda_2, \lambda_3, \lambda_5$, and λ_6 are complex, hence, $\mathrm{v}_2, \mathrm{v}_3, \mathrm{v}_5$ and v_6 are complex. Besides, $\mathbf{v}_3 = \mathbf{v}_2^{\dagger}$ and $\mathbf{v}_6 = \mathbf{v}_5^{\dagger}$, since $\lambda_3 = \lambda_2^{\dagger}$ and $\lambda_6 = \lambda_5^{\dagger}$, where the symbol † denotes the conjugate. Therefore, for Case one the general solution to equation (3.15) can be obtained as follows:

$$\bar{\boldsymbol{\psi}}(\xi, z, s) = \sum_{i=1,4} E_i \mathbf{v}_i e^{\lambda_i z} + E_2' \mathbf{h}_2 e^{-\gamma_2 z} + E_3' \mathbf{h}_3 e^{-\gamma_3 z} + E_5' \mathbf{h}_5 e^{\gamma_2 z} + E_6' \mathbf{h}_6 e^{\gamma_3 z}, \tag{3.23}$$

in which $\gamma_2 = \gamma_3$, which denote the real part of the Eigenvalue and E_i' $(i = 2,3,5,6)$ are arbitrary constants. The vectors $\mathbf{h}_i$ $(i = 2,3,5,6)$ in equation (3.23) are expressed as follows:

$$\mathbf{h}_2 = \cos\alpha z\, \mathbf{v}_2^{(R)} + \sin\alpha z\, \mathbf{v}_2^{(I)},\ \mathbf{h}_3 = -\sin\alpha z\, \mathbf{v}_2^{(R)} + \cos\alpha z\, \mathbf{v}_2^{(I)},$$

$$\mathbf{h}_5 = \cos\alpha z\, \mathbf{v}_5^{(R)} - \sin\alpha z\, \mathbf{v}_5^{(I)},\ \mathbf{h}_6 = \sin\alpha z\, \mathbf{v}_5^{(R)} + \cos\alpha z\, \mathbf{v}_5^{(I)}, \tag{3.24}$$

with $\mathbf{v}_i^{(R)}$ and $\mathbf{v}_i^{(I)}$ $(i = 2,5)$ being the real and imaginary part of $\mathbf{v}_i$ $(i = 2,5)$, respectively.

Case two

For the case where Δ is negative, all the three roots (y_1, y_2 and y_3) of equation (3.19) are distinct and real. In the scenario where y_1, y_2 and y_3 are all positive, then all the Eigenvalues and their corresponding Eigenvectors of the matrix $\bar{\mathbf{A}}(\xi, s)$ are all real. In this case, the general solution to equation (3.15) can simply be obtained as:

$$\bar{\boldsymbol{\psi}}(\xi, z, s) = \sum_{i=1}^{6} E_i \mathbf{v}_i e^{\lambda_i z}, \tag{3.25}$$

where $\mathbf{v}_i$ $(i=1,2,...,6)$ denotes the Eigenvectors of the matrix $\bar{\mathbf{A}}(\xi,s)$. The Eigenvalues in above equation (3.25) can be obtained as: $\lambda_1=-\sqrt{y_1}=-\gamma_1$, $\lambda_2=-\sqrt{y_2}=-\gamma_2$, $\lambda_3=-\sqrt{y_3}=-\gamma_3$, $\lambda_4=-\lambda_1=\gamma_1$, $\lambda_5=-\lambda_2=\gamma_2$, $\lambda_6=-\lambda_3=\gamma_3$. However, with a negative Δ, it is also possible that y_2 and y_3 might be negative. In this scenario, the Eigenvalues of the matrix $\bar{\mathbf{A}}(\xi,s)$ are as follows:

$$\lambda_1=-\sqrt{y_1}=-\gamma_1,\ \lambda_2=-\sqrt{y_2}=-\gamma_2+\mathrm{i}\alpha_2,\ \lambda_3=-\sqrt{y_3}=-\gamma_3+\mathrm{i}\alpha_3,$$

$$\lambda_4=-\lambda_1=\gamma_1,\ \lambda_5=-\lambda_2=\gamma_2\text{-}\mathrm{i}\alpha_2,\ \lambda_6=-\lambda_3=-\gamma_3+\mathrm{i}\alpha_3, \tag{3.26}$$

where, the real parts $\gamma_2=\gamma_3=0$ and the imaginary part $\alpha_1=0$. Therefore, in this particular case, the general solution to equation (3.15) can be expressed as:

$$\bar{\boldsymbol{\psi}}(\xi,z,s)=\sum_{i=1,4}E_i\mathbf{v}_ie^{\lambda_i z}+E_2''\,\mathbf{h}_2e^{-\gamma_2 z}+E_3''\,\mathbf{h}_3e^{-\gamma_3 z}+E_5''\,\mathbf{h}_5e^{\gamma_2 z}+E_6''\,\mathbf{h}_6e^{\gamma_3 z}, \tag{3.27}$$

where E_i'' $(i=2,3,5,6)$ denote the arbitrary constants and the vectors $\mathbf{h}_i$ $(i=2,3,5,6)$ are given by:

$$\mathbf{h}_2=\cos\alpha_2 z\,\mathbf{v}_2^{(R)}-\sin\alpha z\,\mathbf{v}_2^{(I)},\ \mathbf{h}_3=\cos\alpha_3 z\,\mathbf{v}_3^{(R)}-\sin\alpha_3 z\mathbf{v}_3^{(I)},$$

$$\mathbf{h}_5=\cos\alpha_2 z\,\mathbf{v}_2^{(R)}+\sin\alpha z\,\mathbf{v}_2^{(I)},\ \mathbf{h}_6=\sin\alpha_3 z\,\mathbf{v}_3^{(R)}+\cos\alpha z\,\mathbf{v}_3^{(I)}, \tag{3.28}$$

with $\mathbf{v}_i^{(R)}$ and $\mathbf{v}_i^{(I)}$ $(i=2,5)$ being the real and imaginary part of $\mathbf{v}_i$ $(i=2,5)$, respectively.

Case three

In the case where $\Delta=0$ $(p \neq 0, q \neq 0)$, equation (3.19) has one real single root y_1 and one double root, i.e., $y_2 = y_3$. Thus, the eigenvalues of the matrix $\bar{\mathbf{A}}(\xi, s)$ have the following forms:

$$\lambda_1 = -\sqrt{y_1} = -\gamma_1,\ \lambda_2 = -\sqrt{y_2} = -\gamma_2,\ \lambda_3 = -\sqrt{y_3} = -\gamma_3,$$

$$\lambda_4 = -\lambda_1 = \gamma_1,\ \lambda_5 = -\lambda_2 = \gamma_2,\ \lambda_6 = -\lambda_3 = \gamma_3, \tag{3.29}$$

in which $\lambda_2 = \lambda_3$ and $\lambda_5 = \lambda_6 = -\lambda_2$ since the two roots y_2 and y_3 are equal. Hence, the general solution to equation (3.15) can thus be given as follows:

$$\bar{\boldsymbol{\psi}}(\xi, z, s) = \sum_{i=1,4} E_i \mathbf{v}_i e^{\lambda_i z} + \sum_{i=2,3,5,6} E_i''' \mathbf{k}_i e^{\lambda_i z}, \tag{3.30}$$

were, E_i''' $(i = 2,3,5,6)$ are the arbitrary constants and the vectors $\mathbf{k}_i$ $(i = 2,3,5,6)$ are obtained from the following expressions:

$$\mathbf{k}_2 = \mathbf{v}_{10}^{(-)} + z\mathbf{v}_{11}^{(-)},\ \mathbf{k}_3 = \mathbf{v}_{20}^{(-)} + z\mathbf{v}_{21}^{(-)},$$

$$\mathbf{k}_5 = \mathbf{v}_{10}^{(+)} + z\mathbf{v}_{11}^{(+)},\ \mathbf{k}_6 = \mathbf{v}_{20}^{(+)} + z\mathbf{v}_{21}^{(+)}, \tag{3.31}$$

in which the vectors $\mathbf{v}_{ij}^{(-)}$ and $\mathbf{v}_{ij}^{(+)}$ $(i = 1,2;\ j = 0,1)$ are determined by the following equations:

$$\left[\bar{\mathbf{A}}(\xi, s) - \lambda_2 \mathbf{I}_{6\times6}\right]^2 \mathbf{v}_{j0}^{(-)} = \mathbf{0},\ \mathbf{v}_{j1}^{(-)} = \left[\bar{\mathbf{A}}(\xi, s) - \lambda_2 \mathbf{I}_{6\times6}\right] \mathbf{v}_{j0}^{(-)},\ j = 1,2,$$

$$\left[\bar{\mathbf{A}}(\xi, s) + \lambda_2 \mathbf{I}_{6\times6}\right]^2 \mathbf{v}_{j0}^{(+)} = \mathbf{0},\ \mathbf{v}_{j1}^{(+)} = \left[\bar{\mathbf{A}}(\xi, s) + \lambda_2 \mathbf{I}_{6\times6}\right] \mathbf{v}_{j0}^{(+)},\ j = 1,2.$$

It is noted that Case three corresponds to an isotropic saturated soil, while, the other two cases (case one and two) correspond to an anisotropic saturated soil.

In summary, for all the three above-mentioned cases, the general solution to equation (3.15) can be represented uniformly in the following form:

$$\bar{\boldsymbol{\psi}}(\xi,\mathrm{z},\mathrm{s}) = \sum_{i=1}^{3} E_i^* \mathbf{V}_i e^{-\gamma_i z} + \sum_{i=4}^{6} E_i^* \mathbf{V}_i e^{\gamma_{i-3} z} \ ,$$

(3.32)

in which E_i^* $(i=1\sim 6)$ are referred to as the arbitrary constants; γ_i and $\mathbf{V}_i$ $(i=1\sim 6)$ are the ith real part of the Eigen value and the Eigenvector of the matrix $\bar{\mathbf{A}}(\xi,s)$, respectively. Note that the concrete representation of the above equation (3.32) depends on the property of the roots for equation (3.19) as described in the aforementioned three cases.

3.3 The reflection and transmission matrices (RTMs) for the layered half-space TISS subject to a vertical point force

In this section, based on the general solution established in the previous section, the reflection and transmission matrices (RTMs) corresponding to the static wave vector associated to arbitrary points on the layered TISS half-space are demonstrated briefly.

3.3.1 The state and static wave vectors and the corresponding transfer matrices

For all the three cases mentioned in the previous section, the general solution to equation (3.15) can also be expressed in the following form:

$$\bar{\boldsymbol{\psi}}(\xi,\mathrm{z},\mathrm{s}) = \mathbf{M}(\xi,z,s)\mathbf{w}(\xi,z,s)\ ,\ \mathbf{w}(\xi,z,s) = \left\{\mathbf{w}_d^T(\xi,z,s),\mathbf{w}_u^T(\xi,z,s)\right\}^T , \qquad (3.33)$$

where the six-dimensional vector $\mathbf{w}(\xi,z,s)$ denotes the static wave vector, in which $\mathbf{w}_d(\xi,z,s) = \left\{E_1 e^{-\gamma_1 z}\ E_2^* e^{-\gamma_2 z}\ E_3^* e^{-\gamma_3 z}\right\}^T$ and $\mathbf{w}_u(\xi,z,s) = \left\{E_4 e^{\gamma_1 z}\ E_5^* e^{\gamma_2 z}\ E_6^* e^{\gamma_3 z}\right\}^T$, where each contains three negative and positive exponential terms and corresponding arbitrary constants and they denote the down-going and up-going wave vectors, respectively. In the above equation (3.33), the state vector is related to the static wave vector by the 6×6 transform matrix $\mathbf{M}(\xi,z,s)$, which according to equation (3.32) can be expressed as follows:

$$\mathbf{M}(\xi,z,s)=\left[\mathbf{V}_1\,\mathbf{V}_2\,\mathbf{V}_3\,\mathbf{V}_4\,\mathbf{V}_5\,\mathbf{V}_6\ \right]. \tag{3.34}$$

For simplification purposes, it is noted that the parameters ξ and s will be omitted in the subsequent analysis. Thus, referring to the decomposition of the state and wave vectors, the transform matrix can be decomposed as follows accordingly:

$$\mathbf{M}(z)=\begin{bmatrix}\mathbf{D}_d(z) & \mathbf{D}_u(z)\\ \mathbf{S}_d(z) & \mathbf{S}_u(z)\end{bmatrix}, \tag{3.35}$$

where $\mathbf{D}_d(z)$ and $\mathbf{D}_u(z)$ are the 3×3 sub-matrices of $\mathbf{M}(z)$ that combine the down-going static wave vectors into $\bar{\mathbf{u}}$, while $\mathbf{S}_d(z)$ and $\mathbf{S}_u(z)$ combine up-going static wave vectors into $\bar{\mathbf{f}}$.

At this step, for a scenario where both plane z_R and z are located in the same soil layer and z is assumed to be below z_R, then, according to equation (3.33), the static wave vectors $\mathbf{w}(z_R)$ at the plane z_R can be obtained as:

$$\mathbf{w}(z_R)=\left\{\mathbf{w}_d^T(z_R)\,\mathbf{w}_u^T(z_R)\right\}^T, \tag{3.36}$$

with $\mathbf{w}_d(z_R)=\left\{E_1e^{-\gamma_1 z_R}\ E_2^* e^{-\gamma_2 z_R}\ E_3^* e^{-\gamma_3 z_R}\right\}^T$ and $\mathbf{w}_u(z_R)=\left\{E_4e^{\gamma_1 z_R}\ E_5^* e^{\gamma_2 z_R}\ E_6^* e^{\gamma_3 z_R}\right\}^T$. While introducing the wave vector transfer matrix $\mathbf{T}^{(W)}(z,z_R)$, the static wave vectors $\mathbf{w}(z)$ at the plane z can be obtained by the following relation:

$$\mathbf{w}(z)=\mathbf{T}^{(W)}(z,z_R)\mathbf{w}(z_R), \tag{3.37}$$

where $\mathbf{T}^{(W)}(z,z_R)=\mathbf{\Lambda}(z-z_R)$ is referred to as the wave vector transfer matrix relating the static wave vector $\mathbf{w}(z)$ at the plane z to the wave vector $\mathbf{w}(z_R)$ at the plane z_R, In which

$$\mathbf{\Lambda}(z-z_R)=\begin{bmatrix}\mathbf{\Omega}(z-z_R) & \mathbf{0}\\ \mathbf{0} & \mathbf{\Omega}^{-1}(z-z_R)\end{bmatrix},\ \mathbf{\Omega}(z-z_R)=\begin{bmatrix}\omega_{11} & 0 & 0\\ 0 & \omega_{22} & 0\\ 0 & 0 & \omega_{33}\end{bmatrix},$$

$$\omega_{11}=e^{-(z-z_R)\gamma_1},\ \omega_{22}=e^{-(z-z_R)\gamma_2},\ \omega_{33}=e^{-(z-z_R)\gamma_3}. \tag{3.38}$$

Besides, with the use of equations (3.33) , (3.37) and (3.38), the state vectors at the planes z and z_R can also be related as follows:

$$\bar{\boldsymbol{\psi}}(z)=\mathbf{M}(z)\mathbf{w}(z)=\mathbf{M}(z)\mathbf{\Lambda}(z-z_R)\mathbf{M}^{-1}(z_R)\mathbf{M}(z_R)\mathbf{w}(z_R)$$

$$=\mathbf{M}(z)\mathbf{\Lambda}(z-z_R)\mathbf{M}^{-1}(z_R)\bar{\boldsymbol{\psi}}(z_R)=\mathbf{M}(z)\mathbf{T}^{(W)}(z,z_R)\mathbf{M}^{-1}(z_R)\bar{\boldsymbol{\psi}}(z_R). \tag{3.39}$$

Hence, introducing the state vector transfer matrix $\mathbf{T}^{(S)}(z,z_R)$ which relates the state vector $\bar{\boldsymbol{\psi}}(z)$ at the plane z to the state vector $\bar{\boldsymbol{\psi}}(z_R)$ at the plane z_R, equation (3.39) is reformulated as follows:

$$\bar{\boldsymbol{\psi}}(z)=\mathbf{T}^{(S)}(z,z_R)\bar{\boldsymbol{\psi}}(z_R), \tag{3.40}$$

in which $\mathbf{T}^{(S)}(z,z_R)=\mathbf{M}(z)\mathbf{\Lambda}(z-z_R)\mathbf{M}^{-1}(z_R)=\mathbf{M}(z)\mathbf{T}^{(W)}(z,z_R)\mathbf{M}^{-1}(z_R)$.

As mentioned earlier, plane z_R and z belong to the same soil layer, thus the wave and state vector transfer matrix defined in equation (3.37) and (3.40), respectively can be used relating two arbitrary planes in the same soil layer. However, for any two planes that belong to two different soil layers of the layered half-space, equations (3.37) and (3.40) cannot be applied directly.

Suppose that the ith interface is free of any external sources and in addition, the layered saturated soil is fully bound and permeable at all the interfaces. Hence, the following continuity condition holds at the ith interface:

$$\bar{\boldsymbol{\psi}}(z_i^{(-)}) = \bar{\boldsymbol{\psi}}(z_i^{(+)}), \tag{3.41}$$

where z_i denotes the vertical coordinate of the ith interface and $z_i^{(-)}$ and $z_i^{(+)}$ denotes the vertical coordinate of a plane approaching the ith interface from the upper side and downside, respectively. By using equations (3.39) and (3.41), the following equation is obtained:

$$\mathbf{w}(z_i^{(+)}) = \mathbf{T}^{(W)}(z_i^{(+)}, z_i^{(-)})\mathbf{w}(z_i^{(-)}), \ \mathbf{T}^{(W)}(z_i^{(+)}, z_i^{(-)}) = \mathbf{M}^{-1}(z_i^{(+)})\mathbf{M}\ (z_i^{(-)}), \ i = 1 \sim N, \tag{3.42}$$

where $\mathbf{T}^{(W)}(z_i^{(+)}, z_i^{(-)})$ denotes the transfer matrix at the ith interface for the wave vector; $\mathbf{M}\ (z_i^{(-)})$ and $\mathbf{M}\ (z_i^{(+)})$ are the transform matrices between the state and wave vectors at the coordinates $z_i^{(-)}$ and $z_i^{(+)}$, respectively. It is noted, however, as the transform matrix $\mathbf{M}(z_i)$ depends on both the vertical coordinate and the material parameters associated with the coordinate, $\mathbf{M}\ (z_i^{(-)})$ and $\mathbf{M}\ (z_i^{(+)})$ depend on the material parameters of the L_ith and L_{i+1}th layers, respectively, and hence they are usually not equal. Thus, $\mathbf{T}^{(W)}(z_i^{(+)}, z_i^{(-)})$ is not usually equivalent to the identity matrix. By using equations (3.40) and (3.41), the transfer matrix linking two state vectors of two arbitrary planes of the layered TISS can be obtained. Also, with equations (3.37) and (3.42), the transfer matrix linking two wave vectors associated with two arbitrary planes of the layered TISS is also obtainable.

3.3.2 The expressions for the RTMs of the layered half-space TISS

In this section, two examples are used to illustrate how the RTMs of the layered half-space TISS can be related to the transfer matrices of the wave vectors of the layered TISS introduced in the previous section.

First, suppose two arbitrary coordinates z_α and z_β where $(z_\alpha < z_\beta)$ and their respective wave vectors $\mathbf{w}(z_\alpha)$ and $\mathbf{w}(z_\beta)$. Since z_α and z_β are arbitrary, the soil layer $L_S(z_\beta, z_\alpha)$ may be inhomogeneous with an arbitrary number of interfaces. Thus, considering the definition for the down-going and up-going wave vectors in equation (3.33), the wave vectors $\mathbf{w}(z_\beta)$ and $\mathbf{w}(z_\alpha)$ can be related as follows:

$$\begin{Bmatrix} \mathbf{w}_d(z_\beta) \\ \mathbf{w}_u(z_\beta) \end{Bmatrix} = \begin{bmatrix} \mathbf{T}_{dd}^{(W)}(z_\beta, z_\alpha) & \mathbf{T}_{du}^{(W)}(z_\beta, z_\alpha) \\ \mathbf{T}_{ud}^{(W)}(z_\beta, z_\alpha) & \mathbf{T}_{uu}^{(W)}(z_\beta, z_\alpha) \end{bmatrix} \begin{Bmatrix} \mathbf{w}_d(z_\alpha) \\ \mathbf{w}_u(z_\alpha) \end{Bmatrix}, \tag{3.43}$$

where $\mathbf{w}_d(z_\alpha)$ and $\mathbf{w}_u(z_\alpha)$ denote the down-going and up-going wave vectors at the plane z_α; $\mathbf{w}_d(z_\beta)$ and $\mathbf{w}_u(z_\beta)$ are those at the plane z_β; $\mathbf{T}_{dd}^{(W)}$, $\mathbf{T}_{du}^{(W)}$, $\mathbf{T}_{ud}^{(W)}$ and $\mathbf{T}_{uu}^{(W)}$ are the 3×3 sub-matrices of the wave vector transfer matrix $\mathbf{T}^{(W)}(z_\beta, z_\alpha)$. By reformulating the above equation (3.43), the RTMs for the soil layer $L_S(z_\beta, z_\alpha)$ can be introduced and obtained, assuming the wave vector transfer matrix $\mathbf{T}^{(W)}(z_\beta, z_\alpha)$ to be known a priori. Thus, equation (3.43) can be rewritten as follows:

$$\begin{Bmatrix} \mathbf{w}_u(z_\alpha) \\ \mathbf{w}_d(z_\beta) \end{Bmatrix} = \begin{bmatrix} \mathbf{R}_d(z_\beta, z_\alpha) & \mathbf{T}_u(z_\beta, z_\alpha) \\ \mathbf{T}_d(z_\beta, z_\alpha) & \mathbf{R}_u(z_\beta, z_\alpha) \end{bmatrix} \begin{Bmatrix} \mathbf{w}_d(z_\alpha) \\ \mathbf{w}_u(z_\beta) \end{Bmatrix},$$

(3.44)

in which $\mathbf{R}_d(z_\beta, z_\alpha)$ and $\mathbf{R}_u(z_\beta, z_\alpha)$ are referred to as the reflection matrices of the soil layer $L(z_\beta, z_\alpha)$ for the down-going and up-going wave vectors; while, $\mathbf{T}_d(z_\beta, z_\alpha)$ and $\mathbf{T}_u(z_\beta, z_\alpha)$ are the transmission matrices of $L_S(z_\beta, z_\alpha)$ for the down-going and up-going wave vectors, respectively. As noted above, if the four sub-matrices of the wave vector transfer matrix $\mathbf{T}^{(W)}(z_\beta, z_\alpha)$ in equation (3.43) are known in advance, then, the RTMs defined in equation (3.44) are obtainable by the following equations [64] :

$$\mathbf{R}_d(z_\beta, z_\alpha) = -\,\mathbf{T}_{uu}^{(W)-1}(z_\beta, z_\alpha)\mathbf{T}_{ud}^{(W)-1}(z_\beta, z_\alpha),\ \mathbf{R}_u(z_\beta, z_\alpha) = \mathbf{T}_{du}^{(W)}(z_\beta, z_\alpha)\mathbf{T}_{uu}^{(W)-1}(z_\beta, z_\alpha),$$

$$\mathbf{T}_d(z_\beta, z_\alpha) = \mathbf{T}_{dd}^{(W)}(z_\beta, z_\alpha) - \mathbf{T}_{du}^{(W)}(z_\beta, z_\alpha)\mathbf{T}_{uu}^{(W)-1}(z_\beta, z_\alpha)\mathbf{T}_{ud}^{(W)}(z_\beta, z_\alpha),$$

$$\mathbf{T}_u(z_\beta, z_\alpha) = \mathbf{T}_{uu}^{(W)-1}(z_\beta, z_\alpha). \tag{3.45}$$

For the second example, suppose three state vectors $\bar{\boldsymbol{\psi}}(z_\alpha)$, $\bar{\boldsymbol{\psi}}(z_\beta)$ and $\bar{\boldsymbol{\psi}}(z_\gamma)$ for planes z_α, z_β and z_γ $(z_\alpha < z_\beta < z_\gamma)$, respectively, and their corresponding wave vectors $\mathbf{w}(z_\alpha)$, $\mathbf{w}(z_\beta)$ and $\mathbf{w}(z_\gamma)$, receptively. Noticeably, the state vectors $\bar{\boldsymbol{\psi}}(z_\alpha)$ and $\bar{\boldsymbol{\psi}}(z_\gamma)$ can be related as follows:

$$\bar{\boldsymbol{\psi}}(z_\gamma) = \mathbf{T}^{(S)}(z_\gamma, z_\alpha)\bar{\boldsymbol{\psi}}(z_\alpha) = \mathbf{T}^{(S)}(z_\gamma, z_\beta)\mathbf{T}^{(S)}(z_\beta, z_\alpha)\bar{\boldsymbol{\psi}}(z_\alpha), \tag{3.46}$$

and the wave vectors $\bar{\mathbf{w}}(z_\alpha)$ and $\bar{\mathbf{w}}(z_\gamma)$ at the planes z_α and z_γ, respectively have the following relation:

$$\mathbf{w}(z_\gamma) = \mathbf{T}^{(W)}(z_\gamma, z_\alpha)\mathbf{w}(z_\alpha) = \mathbf{T}^{(W)}(z_\gamma, z_\beta)\mathbf{T}^{(W)}(z_\beta, z_\alpha)\mathbf{w}(z_\alpha)\,. \tag{3.47}$$

At this step, it is worth noting that the RTMs for the soil layer $L_S(z_\gamma, z_\alpha)$ can be obtained by combining the RTMs for the soil layers $L_S(z_\beta, z_\alpha)$ and $L_S(z_\gamma, z_\beta)$. Therefore, by using equation (3.45) and assuming that the RTMs of the soil layers $L_S(z_\beta, z_\alpha)$ and $L_S(z_\gamma, z_\beta)$ are known in advance, the RTMs of the soil layer $L_S(z_\gamma, z_\alpha)$ can thus be gotten as follows [64]:

$$\mathbf{R}_d(z_\gamma, z_\alpha) = \mathbf{R}_d(z_\beta, z_\alpha) + \mathbf{T}_u(z_\beta, z_\alpha)\mathbf{\Gamma}_a^{-1}(z_\gamma, z_\beta, z_\alpha)\mathbf{R}_d(z_\gamma, z_\beta)\mathbf{T}_d(z_\beta, z_\alpha)\,,$$

$$\mathbf{R}_u(z_\gamma, z_\alpha) = \mathbf{R}_u(z_\gamma, z_\beta) + \mathbf{T}_d(z_\gamma, z_\beta)\mathbf{R}_u(z_\beta, z_\alpha)\mathbf{\Gamma}_a^{-1}(z_\gamma, z_\beta, z_\alpha)\mathbf{T}_u(z_\gamma, z_\beta)\,,$$

$$\mathbf{T}_d(z_\gamma, z_\alpha) = \mathbf{T}_d(z_\gamma, z_\beta)\mathbf{\Gamma}_b^{-1}(z_\gamma, z_\beta, z_\alpha)\mathbf{T}_d(z_\beta, z_\alpha)\,,$$

$$\mathbf{T}_u(z_\gamma, z_\alpha) = \mathbf{T}_u(z_\beta, z_\alpha)\mathbf{\Gamma}_a^{-1}(z_\gamma, z_\beta, z_\alpha)\mathbf{T}_u(z_\gamma, z_\beta)\,,$$

$$\mathbf{\Gamma}_a(z_\gamma, z_\beta, z_\alpha) = \mathbf{I}_{3\times3} - \mathbf{R}_d(z_\gamma, z_\beta)\mathbf{R}_u(z_\beta, z_\alpha)\,,$$

$$\mathbf{\Gamma}_b(z_\gamma, z_\beta, z_\alpha) = \mathbf{I}_{3\times3} - \mathbf{R}_u(z_\beta, z_\alpha)\mathbf{R}_d(z_\gamma, z_\beta)\,, \tag{3.48}$$

where $\mathbf{I}_{3\times3}$ is the 3×3 identity matrix.

3.4 Solution of the layered half-space TISS obtained by the RTM method

In this section, the solutions for the layered half-space TISS subjected to external sources are established based on the RTMs for the layered TISS proposed in the previous section.

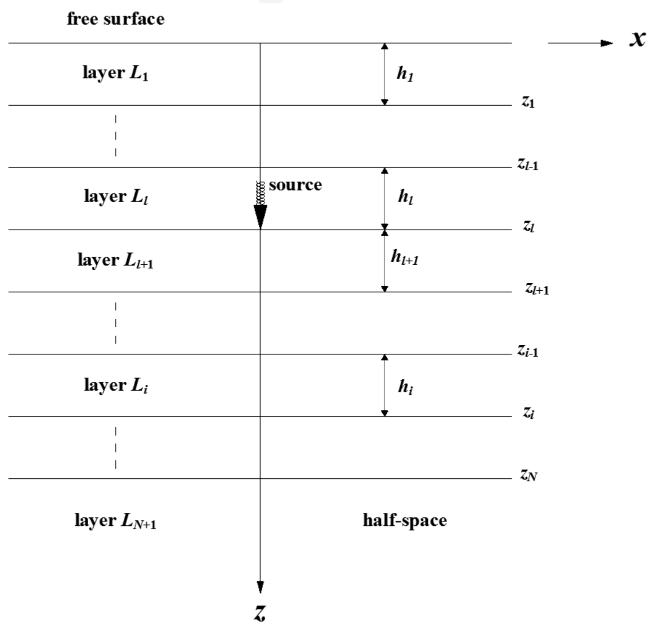

Figure 3. 1 Schematic of the layered half-space TISS with $N+1$ layers subjected to an external point source

Figure 3.1 illustrates the layered saturated soil with $N+1$ layers subjected to a source at the interface between the L_lth and L_{l+1}th layers. Due to the presence of the source, the layered TISS can then be separated into two parts. However, in case the source is applied in a homogeneous layer rather than at a soil interface, the homogeneous layer can be divided into two layers artificially by the source plane.

Since the interface between the layers L_l and L_{l+1} is subjected to a source, the following jump condition for the state vector holds:

$$\mathbf{M}(z_l^{(+)})\mathbf{w}(z_l^{(+)}) - \mathbf{M}(z_l^{(-)})\mathbf{w}(z_l^{(-)}) = \bar{\boldsymbol{\psi}}_s(z_l)\Big|_-^+ , \qquad (3.49)$$

where $\bar{\boldsymbol{\psi}}_s(z_l)\Big|_-^+$ denotes the jump of the state vector at the source plane. Suppose that at the point $(r,z)=(0,z_l)$ there is applied a vertical force Q along the z -direction, then all the quantities in the state vector as defined in equation (3.15) except $\bar{\sigma}_{zz}^{(0)}$ are continuous when across the source plane. Thus, one has:

$$\boldsymbol{\psi}_s(z_l)\Big|_-^+ = \left\{\mathbf{u}^T\Big|_-^+ \ \mathbf{f}^T\Big|_-^+\right\}^{\mathrm{T}},\ \mathbf{u}\Big|_-^+ = \mathbf{0},\ \mathbf{f}\Big|_-^+ = \left\{\frac{Q\delta(r)}{\pi r}H(t), 0, 0\right\}^{\mathrm{T}},$$

$$\bar{\boldsymbol{\psi}}_s(z_l)\Big|_-^+ = \left\{\bar{\mathbf{u}}^T\Big|_-^+ \ \bar{\mathbf{f}}^T\Big|_-^+\right\}^{\mathrm{T}},\ \bar{\mathbf{u}}\Big|_-^+ = \mathbf{0},\ \bar{\mathbf{f}}\Big|_-^+ = \left\{\frac{Q}{\pi s}, 0, 0\right\}^{\mathrm{T}}, \qquad (3.50)$$

where $\delta(*)$ and $H(*)$ are the Dirac and Heaviside functions, respectively. In order to apply the fundamental solution in the next Chapter 4, the radius R of the circular path should be taken into account, thus, for a circular uniform patch load with the centre located at the point $(r,z)=(0,z_l)$ and the resultant force Q in the z -direction, the jump of the state vector at the source plane has the following expression:

$$\mathbf{u}\Big|_-^+ = \mathbf{0},\ \mathbf{f}\Big|_-^+ = \left\{\frac{Q}{A}H(t), 0, 0\right\}^{\mathrm{T}},\ \bar{\mathbf{u}}\Big|_-^+ = \mathbf{0},\ \bar{\mathbf{f}}\Big|_-^+ = \left\{\frac{QRJ_1(R\xi)}{A\xi s}, 0, 0\right\}^{\mathrm{T}}, \qquad (3.51)$$

in which R and A represents the radius and the area of the circular patch load, respectively.

By considering equation (3.35), equation (3.49) can be reformulated as:

$$\begin{bmatrix} D_d(z_l^{(+)}) & D_u(z_l^{(+)}) \\ S_d(z_l^{(+)}) & S_u(z_l^{(+)}) \end{bmatrix} \begin{Bmatrix} \mathbf{w}_d(z_l^{(+)}) \\ \mathbf{w}_u(z_l^{(+)}) \end{Bmatrix} - \begin{bmatrix} D_d(z_l^{(-)}) & D_u(z_l^{(-)}) \\ S_d(z_l^{(-)}) & S_u(z_l^{(-)}) \end{bmatrix} \begin{Bmatrix} \mathbf{w}_d(z_l^{(-)}) \\ \mathbf{w}_u(z_l^{(-)}) \end{Bmatrix} = \bar{\boldsymbol{\psi}}_s(z_l)\Big|_-^+ . \qquad (3.52)$$

Assuming that for the soil layer $L_S(z_l^{(-)}, z_0)$, the reflection matrix for the up-going wave vector is $\mathbf{R}_u(z_l^{(-)}, z_0)$, where z_0 is referred to as the vertical coordinate at the surface of the layered half-space TISS, then the following equation for the wave vector $\mathbf{w}_d(z_l^{(-)})$ can be obtained:

$$\mathbf{w}_d(z_l^{(-)}) = \mathbf{R}_u(z_l^{(-)}, z_0)\mathbf{w}_u(z_l^{(-)}). \tag{3.53}$$

Similarly, supposing that $\mathbf{R}_d(\infty, z_l^{(+)})$ is the reflection matrix of the soil laye $L_S(\infty, z_l^{(+)})$ for the down-going wave vector, then, the wave vector $\mathbf{w}_u(z_l^{(+)})$ can also be represented by:

$$\mathbf{w}_u(z_l^{(+)}) = \mathbf{R}_d(\infty, z_l^{(+)})\mathbf{w}_d(z_l^{(+)}). \tag{3.54}$$

Thus, Employing equations (3.53) and (3.54), equation (3.52) yields the following equation for the wave vectors $\mathbf{w}_d(z_l^{(+)})$ and $\mathbf{w}_u(z_l^{(-)})$:

$$\begin{bmatrix} D_d(z_l^{(+)}) + D_u(z_l^{(+)})\mathbf{R}_d(\infty, z_l^{(+)}) & -D_u(z_l^{(-)}) - D_d(z_l^{(-)})\mathbf{R}_u(z_l^{(-)}, z_0) \\ S_d(z_l^{(+)}) + S_u(z_l^{(+)})\mathbf{R}_d(\infty, z_l^{(+)}) & -S_u(z_l^{(-)}) - S_d(z_l^{(-)})\mathbf{R}_u(z_l^{(-)}, z_0) \end{bmatrix} \begin{Bmatrix} \mathbf{w}_d(z_l^{(+)}) \\ \mathbf{w}_u(z_l^{(-)}) \end{Bmatrix}$$

$$= \bar{\boldsymbol{\Psi}}_s(z_l)\Big|_-^+. \tag{3.55}$$

With the above equation (3.55), the wave vectors $\mathbf{w}_d(z_l^{(+)})$ and $\mathbf{w}_u(z_l^{(-)})$ are obtainable, therefore, the wave vector at the plane $(z_r^{(-)})$ above the source and that at the plane $(z_q^{(+)})$ below the source can be obtained using the RTMs of the corresponding soil layers, i.e.:

$$\begin{Bmatrix} \mathbf{w}_d(z_r^{(-)}) \\ \mathbf{w}_u(z_l^{(-)}) \end{Bmatrix} = \begin{bmatrix} T_{dd}^{(W)}(z_r^{(-)}, z_l^{(-)}) & T_{du}^{(W)}(z_r^{(-)}, z_l^{(-)}) \\ T_{ud}^{(W)}(z_r^{(-)}, z_l^{(-)}) & T_{uu}^{(W)}(z_r^{(-)}, z_l^{(-)}) \end{bmatrix} \begin{Bmatrix} \mathbf{R}_u(z_l^{(-)}, z_0)\mathbf{w}_u(z_l^{(-)}) \\ \mathbf{w}_u(z_l^{(-)}) \end{Bmatrix},$$

$$\begin{Bmatrix} \mathbf{w}_d(z_q^{(+)}) \\ \mathbf{w}_u(z_q^{(+)}) \end{Bmatrix} = \begin{bmatrix} T_{dd}^{(W)}(z_q^{(+)}, z_l^{(+)}) \; T_{du}^{(W)}(z_q^{(+)}, z_l^{(+)}) \\ T_{ud}^{(W)}(z_q^{(+)}, z_l^{(+)}) \; T_{uu}^{(W)}(z_q^{(+)}, z_l^{(+)}) \end{bmatrix} \begin{Bmatrix} \mathbf{w}_d(z_l^{(+)}) \\ \mathbf{R}_d(\infty, z_l^{(+)})\mathbf{w}_d(z_l^{(+)}) \end{Bmatrix}. \tag{3.56}$$

At this step, It is noted that the wave vector transfer matrix $T^{(W)}(z_r^{(-)}, z_l^{(-)})$ in above equation (3.56) is equal to the inverse of the transfer matrix $T^{(W)}(z_l^{(-)}, z_r^{(-)})$ i.e., $T^{(W)-1}(z_r^{(-)}, z_l^{(-)})$, therefore, the sub-matrices of $T^{(W)}(z_r^{(-)}, z_l^{(-)})$ can be represented by the RTMs of the soil layer $L_S(z_l^{(-)}, z_r^{(-)})$. Hence, using equation (3.45), at the plane $z_r^{(-)}$ above the source, the up-going and down-going wave vectors are as follows:

$$\mathbf{w}_d(z_r^{(-)}) = \mathbf{R}_u(z_r^{(-)}, z_0)\mathbf{\Gamma}_a^{-1}(z_l^{(-)}, z_r^{(-)}, z_0)\mathbf{T}_u(z_l^{(-)}, z_r^{(-)})\mathbf{w}_u(z_l^{(-)}),$$

$$\mathbf{w}_u(z_r^{(-)}) = \mathbf{\Gamma}_a^{-1}(z_l^{(-)}, z_r^{(-)}, z_0)\mathbf{T}_u(z_l^{(-)}, z_r^{(-)})\mathbf{w}_u(z_l^{(-)}). \tag{3.57}$$

By using the wave vector at $z_r^{(-)}$ in above equation (3.57), together with the wave vector transfer matrix defined in equation (3.42), the wave vectors at $z_r^{(+)}$ can also be obtained as follows:

$$\mathbf{w}(z_r^{(+)}) = T^{(W)}(z_r^{(+)}, z_r^{(-)})\mathbf{w}(z_r^{(-)}). \tag{3.58}$$

At this step, the wave vector at any random plane z belonging to the layer L_r can be represented, considering the wave vectors at $z_{r-1}^{(+)}$ and $z_r^{(-)}$. i.e.:

$$\begin{Bmatrix} \mathbf{w}_d(z) \\ \mathbf{w}_u(z) \end{Bmatrix} = \begin{bmatrix} \mathbf{\Omega}^{(r)}(z - z_{r-1}) & \mathbf{0} \\ \mathbf{0} & \mathbf{\Omega}^{(r)}(z_r - z) \end{bmatrix} \begin{Bmatrix} \mathbf{w}_d(z_{r-1}^{(+)}) \\ \mathbf{w}_u(z_r^{(-)}) \end{Bmatrix}. \tag{3.59}$$

Likewise, at the plane $z_q^{(+)}$ below the source, the up-going and down-going wave vectors are obtained as follows:

$$\mathbf{w}_d(z_q^{(+)}) = \mathbf{\Gamma}_b^{-1}(\infty, z_q^{(+)}, z_l^{(+)})\mathbf{T}_d(z_q^{(+)}, z_l^{(+)})\mathbf{w}_d(z_l^{(+)}),$$

$$\mathbf{w}_u(z_q^{(+)}) = \mathbf{R}_d(\infty, z_q^{(+)})\mathbf{\Gamma}_b^{-1}(\infty, z_q^{(+)}, z_l^{(+)})\mathbf{T}_d(z_q^{(+)}, z_l^{(+)})\mathbf{w}_d(z_l^{(+)}). \tag{3.60}$$

In a similar way, by using of the wave transfer matrix at the interface z_q the wave vector at $z_q^{(-)}$ can be determined, and the latter can be used together with the waves vectors at $z_{q-1}^{(+)}$ as in equation (3.59) to obtain the wave vector at any arbitrary plane z within the layer L_q. It is noted that the procedure followed to determine the RTMs $R_d(z_l^{(-)}, z_r^{(-)})$ and $\mathbf{T}_u(z_l^{(-)}, z_r^{(-)})$ is slightly different from that to obtain $\mathbf{R}_u(z_r^{(-)}, z_0)$ used in equation (3.57). The RTMs $R_d(z_l^{(-)}, z_r^{(-)})$ and $\mathbf{T}_u(z_l^{(-)}, z_r^{(-)})$ can be obtained by using equation (3.48), repeatedly. And on the other hand, the boundary condition at the surface of the layered half-space soil should be involved in order to obtain $\mathbf{R}_u(z_r^{(-)}, z_0)$. To account on that, if the surface of the layered TISS is assumed to be free of any stress and permeable for the pore fluid, then, at the surface of the layered half-space, the following conditions hold:

$$\bar{\sigma}_{zz}^{(0)} = 0,\ \bar{\tau}_{zr}^{(1)} = 0,\ \bar{p}^{(0)} = 0. \tag{3.61}$$

With equations (3.33) and (3.61), one has:

$$\mathbf{w}_d(z_0^{(+)}) = \mathbf{R}_u(z_0)\mathbf{w}_u(z_0^{(+)}),\ \mathbf{w}_u(z_0^{(+)}) = \mathbf{R}_u^{-1}(z_0)\mathbf{w}_d(z_0^{(+)}),$$

$$\mathbf{R}_u(z_0) = -\mathbf{S}_d^{-1}(z_0^{(+)})\ \mathbf{S}_u(z_0^{(+)}), \tag{3.62}$$

in which $\mathbf{R}_u(z_0)$ is referred to as the reflection matrix of the surface of the layered soil for the up-going wave vector. Since the RTMs of the soil layer $L_S(z_r^{(-)}, z_0^{(+)})$ can be determined via the conventional procedure (section 3.3.2), hence, employing the RTMs of the soil layer $L_S(z_r^{(-)}, z_0^{(+)})$, equation (3.44) can be reformulated as:

$$\begin{Bmatrix} \mathbf{w}_u(z_0^{(+)}) \\ \mathbf{w}_d(z_r^{(-)}) \end{Bmatrix} = \begin{bmatrix} \mathbf{R}_d(z_r^{(-)}, z_0^{(+)}) & \mathbf{T}_u(z_r^{(-)}, z_0^{(+)}) \\ \mathbf{T}_d(z_r^{(-)}, z_0^{(+)}) & \mathbf{R}_u(z_r^{(-)}, z_0^{(+)}) \end{bmatrix} \begin{Bmatrix} \mathbf{w}_d(z_0^{(+)}) \\ \mathbf{w}_u(z_r^{(-)}) \end{Bmatrix}. \tag{3.63}$$

By using equations (3.62) and (3.63), one has the following expression for $\mathbf{w}_d(z_0^{(+)})$:

$$\mathbf{w}_d(z_0^{(+)}) = [\mathbf{R}_u^{-1}(z_0) - \mathbf{R}_d(z_r^{(-)}, z_0^{(+)})]^{-1} \mathbf{T}_u(z_r^{(-)}, z_0^{(+)}) \mathbf{w}_u(z_r^{(-)}), \tag{3.64}$$

And employing equation (3.64) into equation (3.63), $\mathbf{w}_d(z_r^{(-)})$ can be expressed in terms of $\mathbf{w}_u(z_r^{(-)})$ as shown in the following expression:

$$\mathbf{w}_d(z_r^{(-)}) = \{\mathbf{R}_u(z_r^{(-)}, z_0^{(+)}) + \mathbf{T}_d(z_r^{(-)}, z_0^{(+)})[\mathrm{I}_{3\times3} \text{-} \mathbf{R}_d(z_r^{(-)}, z_0^{(+)}) \mathbf{R}_u(z_0)]^{-1}$$

$$\mathbf{T}_u(z_r^{(-)}, z_0^{(+)})\} \mathbf{w}_u(z_r^{(-)}), \tag{3.65}$$

in which $\mathrm{I}_{3\times3}$ denotes the 3×3 identity matrix.

When use equation (3.60) to determine the wave vectors at the soil layers below the source, the RTMs $\mathbf{R}_u(z_q^{(+)}, z_l^{(+)})$ and $\mathbf{T}_d(z_q^{(+)}, z_l^{(+)})$ can be obtained using the conventional procedure. However, when determining $\mathbf{R}_d(\infty, z_q^{(+)})$, the fact that $\mathbf{R}_d(\infty, z_N^{(+)})$ vanishes, resulting in the equivalence of $\mathbf{R}_d(\infty, z_N^{(+)})$ and $\mathbf{R}_d(z_{N+1}^{(+)}, z_q^{(+)})$ should be accounted for.

3.5 Summary

In this chapter, based on the reflection-transmission matrix (RTM) method originally developed for addressing the wave propagation problem in the layered elastic medium, the fundamental solution of a layered Transversely Isotropic Saturated soil (TISS) subjected to a uniform distributed vertical load was obtained. First, a system of partial differential equations was derived based on the governing equations for the TISS in cylindrical coordinate. Using the Hankel–Laplace integral transformation method reviewed in **Chapter 2**, the system of partial differential equations was reduced to a system of ordinary differential equations with which the general solution can be obtained. Later by means of the RTMs for the layered TISS, solutions for the layered TISS subjected to external sources were derived. The fundamental solution for a layered TISS obtained in this chapter will be a useful tool in deriving the integral equation for the pile (**Chapter 4).**

Chapter 4 Analysis of a vertically loaded pile embedded in layered TISS

In this chapter, based on the fundamental solution developed in the previous Chapter 3 together with adopting the fictitious pile method due to Muki & Sternberg [11, 12], the second kind of Fredholm integral equations for the pile embedded in the layered TISS will be derived. It is noted that the fundamental solution for the extended layered TISS is obtained via the RTM method (Chapter 3).

This chapter is organized as follows: First, the Fredholm integral equation of the second kind for the pile in the transformed domain will be developed in which the unknown axial force for the fictitious pile can be determined through numerical calculations (Chapter 5). Once the axial force of the fictitious pile is obtained, the Fredholm integral equation for the real pile axial force can thus be developed in the transformed domain. Finally, the integral equations for other variables such as the real pile displacement and the pile-side soil pore pressure can be obtained, similarly.

It noted, however, the solutions for the real pile axial, displacement and the pile-side soil pore pressure obtained in this chapter are in the Laplace Transformed domain. Thus, numerical methods for the second kind of Fredholm integral equations will be used to obtain the above solutions in the transformed domain, then, with the use of both numerical inversion of the Laplace transform and the Hankel transform (Chapter 2), the time domain solutions can be retrieved.

4.1 Establishment of the Fredholm integral equation for the pile

In this section, the pile subjected to a static vertical load embedded in a two-layered TISS is used as an example to show the procedure to establish the integral equation for the pile. The integral equation for the pile embedded in the layered TISS with arbitrary layers can also be established by following the same procedure. Following Muki's fictitious pile method, the pile-soil system is decomposed into an extended layered half-space TISS and a fictitious pile (Figure 4.1). As noted above, the extended layered TISS is treated as a three-dimensional continuum medium, while the fictitious pile is as a one-dimensional bar. The radius and length of the pile are assumed to be R and L, respectively. According to the fictitious pile method, the Young's modulus of the fictitious pile can be obtained by subtracting the elastic modulus of the soil from the elastic modulus of the real pile, namely

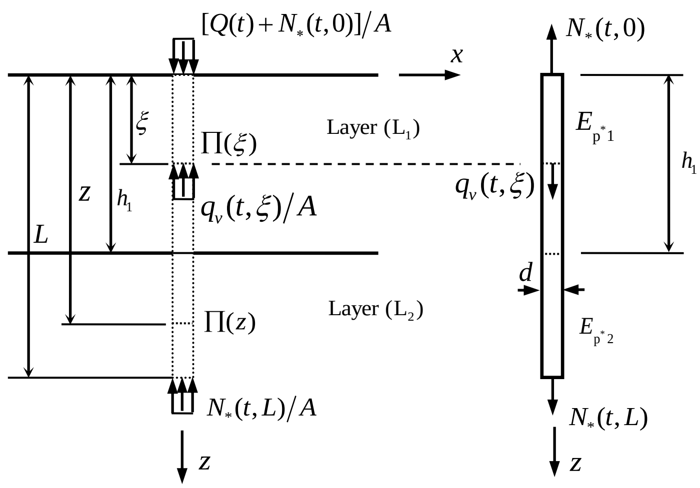

Figure 4. 1 Schematic of (a) the extended saturated half-space and (b) the fictitious pile extracted from the pile-soil system

$$E_{p^*1}=E_p-E_{v1},\ E_{p^*2}=E_p-E_{v2}, \tag{4.1}$$

where E_{p^*1} and E_{p^*2} are the Young's moduli of the segments of the fictitious pile corresponding to the segments of the real pile embedded in the first and second layer, respectively; E_p is the elastic modulus of the real pile; E_{v1} and E_{v2} the vertical Young's moduli of the first and second soil layers, respectively.

As shown in Figure 4.1, it is assumed that the pile is subjected to an external load $Q(t)$ at the top. The axial force of the fictitious pile at time t is $N_*(t,z)$; the vertical distributed load along the fictitious pile at time t is $q_v(t,z)$; and the top and bottom of the fictitious pile are subjected to the forces $N_*(t,0)$ and $N_*(t,L)$ at time t, respectively. The layered TISS is subjected to the reaction force $q_z(t,z)$ from the fictitious pile which is distributed over $\Pi(z)$ uniformly, where $\Pi(z)$ denotes the circular area equivalent to the cross-section area of the pile with the vertical coordinate equal to z and $Q(t)+N_*(t,0)$ as well as $N_*(t,L)$ distributed over $\Pi(0)$ and $\Pi(L)$ uniformly, respectively. According to the equilibrium condition for the fictitious pile, the vertical distributed load along the fictitious pile and the axial force of the fictitious pile at time t have the following relation

$$q_v(t,z) = -\frac{dN_*(t,z)}{dz}. \tag{4.2}$$

According to the aforementioned Muki's fictitious pile method, to accomplish the compatibility between the pile and soil, the axial strain of the fictitious pile is assumed to be equal to the vertical strain of the extended layered TISS along the z-axis, namely

$$\varepsilon_z(t,r,z)\big|_{r=0} = -\varepsilon_{p^*}(t,z), \quad 0 \le z < h, \quad h < z \le L, \tag{4.3}$$

in which $\varepsilon_z(t,r,z)\big|_{r=0}$ represents the vertical strain of the extended TISS half-space at the center of the cross-section $\Pi(z)$ at the time t and $\varepsilon_{p^*}(t,z)$ represents the axial strain of the fictitious pile at the coordinate z at the time t. The axial strain of the fictitious pile at the coordinate z is as follows:

$$\varepsilon_{p*}\left(t,z\right)=\frac{N_{*}(t,z)}{E_{p^{*}i}A}\,,\quad i=1,2\,, \tag{4.4}$$

in which $A=\pi R^2$ represents the cross-section area of the pile

In this study, for generality, the external load acting at the pile top is assumed to be time dependent. Also, during the consolidation process, the axial force of the fictitious pile and the vertical distributed load along the fictitious pile are time-dependent. Hence, the external load, the axial force and the vertical distributed load acting on the fictitious pile can be represented by:

$$Q\left(t\right)=Q\left(0\right)+\int_0^t\dot{Q}\left(\tau,z\right)d\tau\,,\ N_{*}\left(t,z\right)=N_{*}\left(0,z\right)+\int_0^t\dot{N}_{*}\left(\tau,z\right)d\tau\,,$$

$$q_z\left(t,z\right)=q_z\left(0,z\right)+\int_0^t\dot{q}_z\left(\tau,z\right)d\tau\,, \tag{4.5}$$

where the variable with a dot denotes the corresponding time derivative of the variable. Further, for the convenience of the subsequent presentation, the convolution between two arbitrary functions defined in equation (2.13) is adopted herein.

In view of the forces acting at the extended layered TISS, and with the fundamental solution for the layered TISS (Chapter 3), the vertical strain $\varepsilon_z(t,r,z)\big|_{r=0}$ of the extended layered TISS at the center of $\Pi(z)$ can be expressed as follows:

$$\varepsilon_z(t,r,z)\big|_{r=0}=Q(0)\varepsilon_z^{(G)}(t,0,z)+\dot{Q}(t)*\varepsilon_z^{(G)}(t,0,z)+N_{*}(0,0)\varepsilon_z^{(G)}(t,0,z)$$

$$+\dot{N}_{*}(t,0)*\varepsilon_z^{(G)}(t,0,z)-N_{*}(0,L)\varepsilon_z^{(G)}(t,L,z)-\dot{N}_{*}(t,L)*\varepsilon_z^{(G)}(t,L,z)$$

$$-\int_0^L q_v(0,\xi)\varepsilon_z^{(G)}(t,\xi,z)d\xi-\int_0^L\dot{q}_v(t,\xi)*\varepsilon_z^{(G)}(t,\xi,z)d\xi\,, \tag{4.6}$$

in which $N_*(t,0)$ and $N_*(t,L)$ represents the reaction forces corresponding to the forces acting on the top and bottom of the fictitious pile at time t and $\varepsilon_z^{(G)}(t,\xi,z)$ is the vertical strain at $\Pi(z)$ caused by the unit uniformly-distributed load acting over $\Pi(\xi)$.

Using equation (4.2) and integrating equation (4.6) by parts taking into account the discontinuity of $\varepsilon_z^{(G)}(t,\xi,z)$ at $\Pi(z)$ and the jump of the axial force of the virtual pile at the interface between the two soil layers, equation (4.6) can be rewritten as follows:

$$\varepsilon_z(t,r,z)\big|_{r=0} = Q(0)\varepsilon_z^{(G)}(t,0,z) + \dot{Q}(t) * \varepsilon_z^{(G)}(t,0,z)$$

$$+N_*(0,z)[\varepsilon_z^{(G)}(t,z_-,z) - \varepsilon_z^{(G)}(t,z_+,z)] + \dot{N}_*(t,z) * [\varepsilon_z^{(G)}(t,z_-,z) - \varepsilon_z^{(G)}(t,z_+,z)]$$

$$-\int_0^L N_*(0,\xi)\frac{\partial\varepsilon_z^{(G)}(t,\xi,z)}{\partial\xi}d\xi - \int_0^L \dot{N}_*(t,\xi) * \frac{\partial\varepsilon_z^{(G)}(t,\xi,z)}{\partial\xi}d\xi, \tag{4.7}$$

where z_+ and z_- represent the vertical coordinates approaching z from the down and upper sides infinitely. As detailed in the appendixes (II), the expression $\varepsilon_z^{(G)}(t,z_+,z) - \varepsilon_z^{(G)}(t,z_-,z)$ associated with the fundamental solution of the TISS in equation (4.7) can be represented as follows:

$$\varepsilon_z^{(G)}(t,z_+,z) - \varepsilon_z^{(G)}(t,z_-,z) = -\frac{1-v_{hi}-2v_{hvi}v_{vhi}}{AE_{vi}(1-v_{hi})}, \quad i=1,2. \tag{4.8}$$

Applying the above-mentioned pile-soil compatibility condition given by equation (4.3) and using equations (4.4) and (4.7), one has the following second kind Fredholm integral equation for the pile:

$$-\frac{N_*(t,z)}{E_{p^*i}A} + N_*(0,z)[\varepsilon_z^{(G)}(t,z_+,z) - \varepsilon_z^{(G)}(t,z_-,z)] +$$

$$\dot{N}_*(t,z)*[\varepsilon_z^{(G)}(t,z_+,z)-\varepsilon_z^{(G)}(t,z_-,z)]+\int_0^L N_*(0,\xi)\frac{\partial\varepsilon_z^{(G)}(t,\xi,z)}{\partial\xi}d\xi+$$

$$\int_0^L \dot{N}_*(t,\xi)*\frac{\partial\varepsilon_z^{(G)}(t,\xi,z)}{\partial\xi}d\xi=Q(0)\varepsilon_z^{(G)}(t,0,z)+\dot{Q}(t)*\varepsilon_z^{(G)}(t,0,z)\,,\ i=1,2\,. \tag{4.9}$$

To eliminate the time derivatives in equation (4.9), the Laplace transform and the corresponding inverse transform given by equations (2.7) and (2.8), respectively, are introduced. Thus, taking the Laplace transform on equation (4.9) with regard to time t, the transformed second kind Fredholm integral equation of the pile is reduced to:

$$-\frac{\bar{N}_*(s,z)}{E_{p^*i}(z)A}+\left[\bar{\varepsilon}_z^{(G)}(s,z_+,z)-\bar{\varepsilon}_z^{(G)}(s,z_-,z)\right]s\,\bar{N}_*(s,z)$$

$$+\int_0^L s\,\bar{N}_*(s,\xi)\frac{\partial\bar{\varepsilon}_z^{(G)}(s,\xi,z)}{\partial\xi}d\xi=s\,\bar{Q}(s)\bar{\varepsilon}_z^{(G)}(s,0,z)\,,\ i=1,2\,, \tag{4.10}$$

in which the variable with a bar denotes the variable in the Laplace transformed domain.

4.2 Expression for the axial force of the real pile

The axial force $N(t,z)$ of the real pile can be determined by adding the axial force of the fictitious pile to the force acting on $\Pi(z)$. Likewise, it can be represented as follows:

$$N(t,z)=N_*(t,0)-\Big[Q(0)\,f_z^{(G)}(t,0,z)+\dot{Q}(t)*f_z^{(G)}(t,0,z)+N_*(0,0)\,f_z^{(G)}(t,0,z)$$

$$+\dot{N}_*(t,0)*f_z^{(G)}(t,0,z)-N_*(0,L)\,f_z^{(G)}(t,L,z)-\dot{N}_*(t,L)*f_z^{(G)}(t,L,z)$$

$$-\int_0^L q_v(0,\xi)f_z^{(G)}(t,\xi,z)d\xi-\int_0^L \dot{q}_v(t,\xi)*f_z^{(G)}(t,\xi,z)d\xi\Big], \tag{4.11}$$

where $f_z^{(G)}(t,\xi,z)$ is the time-dependent fundamental solution representing the force acting on $\Pi(z)$ caused by a unit uniformly-distributed load acting over $\Pi(\xi)$ with the compressive force considered to be positive. The force $f_z^{(G)}(t,\xi,z)$ can also be obtained by the fundamental solution (Chapter 3). The appearance of the negative sign before the brace is because the sign convention for the normal stress of the soil and that of the pile are opposite.

Similarly, by using equation (4.2) and considering the discontinuity of $f_z^{(G)}(t,\xi,z)$ at $\Pi(z)$ and the jump of the axial force of the fictitious pile at the interface of the soil layers, then integrating by parts equation (4.11), one has the following:

$$N(t,z) = N_*(0,z) + \dot{N}_*(t,z) - Q(0)\, f_z^{(G)}(t,0,z) - \dot{Q}(t) * f_z^{(G)}(t,0,z) +$$

$$N_*(0,z)[\, f_z^{(G)}(t,z_+,z) - f_z^{(G)}(t,z_-,z)] + \dot{N}_*(t,z) * [\, f_z^{(G)}(t,z_+,z) - f_z^{(G)}(t,z_-,z)]$$

$$+\int_0^L N_*(0,\xi)\frac{\partial f_z^{(G)}(t,\xi,z)}{\partial \xi}d\xi + \int_0^L \dot{N}_*(t,\xi) * \frac{\partial f_z^{(G)}(t,\xi,z)}{\partial \xi}d\xi\,. \tag{4.12}$$

Likewise, $f_z^{(G)}(t,z_+,z) - f_z^{(G)}(t,z_-,z)$ associated with the fundamental solution of the TISS has the following property:

$$f_z^{(G)}(t,z_+,z) - f_z^{(G)}(t,z_-,z) = -1\,. \tag{4.13}$$

In a similar way, taking the Laplace transform of equation (4.12) with regard to time t, the axial force of the real pile in a transformed domain can be obtained by the following second kind of the Fredholm integral equation:

$$\bar{N}(s,z) = -s\bar{Q}(s)\,\bar{f}_z^{(G)}(s,0,z) + \int_0^L s\bar{N}_*(s,\xi)\frac{\partial \bar{f}_z^{(G)}(s,\xi,z)}{\partial \xi}d\xi\ . \tag{4.14}$$

4.3 Expression for other variables

In this section, by utilizing of the axial force of the fictitious pile (section 4.1) and the fundamental solution of the layered TISS (Chapter 2) both the vertical displacement of the real pile and the soil pore pressure will be derived. It is, however, necessary to point out that the difference between the derivation of the displacement and the axial force relies on the fact that when the source section $\Pi(\xi)$ passes the receiving section $\Pi(z)$, the corresponding fundamental solution $u_z^{(G)}(t,\xi,z)$ associated with the displacement is continuous, while the fundamental solution $f_z^{(G)}(t,\xi,z)$ associated with the axial force will undergo a jump. Thus, when deriving the expression for the displacement and other continuous variables such as the pore pressure, it is not necessary to break the integral at the receiving section $\Pi(z)$.

Therefore, by following the similar procedure, the vertical displacement of the pile in the Laplace transformed domain can be obtained as follows:

$$\bar{u}_z(s,r,z)\big|_{r=0} = s\bar{Q}(s)\bar{u}_z^{(G)}(s,0,z) - \int_0^L s\bar{N}_*(s,\xi)\frac{\partial \bar{u}_z^{(G)}(s,\xi,z)}{\partial \xi}d\xi\ , \tag{4.15}$$

where $\bar{u}_z(s,r,z)\big|_{r=0}$ is the transformed vertical displacement of the pile; $\bar{u}_z^{(G)}(s,\xi,z)$ is the transformed fundamental solution denoting the vertical displacement at the center of $\Pi(z)$ caused by the unit uniformly-distributed load acting on $\Pi(\xi)$.

The transformed pore pressure in the layered TISS along the side of the pile can also be obtained by means of the axial force of the fictitious pile and the corresponding fundamental solution of the layered TISS as follows:

$$\bar{p}(s,r,z)\big|_{r=R} = s\bar{Q}(s)\,\bar{p}^{(G)}(s,0,z) - \int_0^L s\bar{N}_*(s,\xi)\,\frac{\partial \bar{p}^{(G)}(s,\xi,z)}{\partial \xi}\,d\xi\,, \tag{4.16}$$

in which $\bar{p}\ (s,r,z)\big|_{r=R}$ denotes the pore pressure of the TISS along the side of the pile; $\bar{p}^{(G)}(s,\xi,z)$ is the fundamental solution associated with the transformed pore pressure of the layered TISS at the periphery of $\Pi(z)$ due to the unit uniformly-distributed load acting on $\Pi(\xi)$.

4.4 Numerical solution of the second kind of Fredholm integral equation of the pile embedded in a layered TISS

As mentioned earlier, in this study, the solution technique used to solve the second kind of the Fredholm integral equations (4.10), (4.14), (4.15) and (4.16) mentioned in the previous section, was successfully used by Niumpradit & Karadushi in [20]. However, in this study, due to the layered soil type, the number of soil layers in contact with the pile are taken into account. The integral along the pile embedded in the *i*th soil layer is divided evenly into $N_d^{(i)}$ ($i=1\sim N_L$) number of segments with two end nodes delimiting each segment, in which N_L is the number of the soil layers in contact with the pile. Hence, the total segments used to discretize the pile is equal to $N_d=\sum_{i=1}^{N_L} N_d^{(i)}$. Due to the presence of interfaces between soil layers and the discontinuity of the axial force of the fictitious pile at the interface, two nodes belonging to different segments of the pile and coinciding at a soil interface should be treated as two different nodes. Hence, the total number of nodes is equal to $N_p = N_d + N_L$.

Adopting the method proposed in [20], the integral in equation (4.10) over the segment of the pile with the end nodes z_j and z_{j+1} is evaluated as follows:

$$\int_{z_j}^{z_{j+1}} s\,\bar{N}_*(s,\xi)\frac{\partial\bar{\varepsilon}_z^{(G)}(s,\xi,z)}{\partial\xi}d\xi = \frac{1}{2}s\left[\bar{N}_*\left(s,z_j\right)+\bar{N}_*\left(s,z_{j+1}\right)\right]\times$$

$$\left[\bar{\varepsilon}_z^{(G)}\left(s,z_{j+1},z\right)-\bar{\varepsilon}_z^{(G)}\left(s,z_j,z\right)\right],\ j=1\sim N_d^{(i)}. \tag{4.17}$$

Applying the above equation (4.17) to Fredholm integral equation (4.10), the following system of N_p linear equations can be obtained

$$-\frac{\bar{N}_*(s,z_i)}{E_{p^*}A}+\left[\bar{\varepsilon}_z^{(G)}(s,z_{i+},z_i)-\bar{\varepsilon}_z^{(G)}(s,z_{i-},z_i)\right]s\,\bar{N}_*(s,z_i)+$$

$$\frac{1}{2}\sum_{j=1}^{N_d}s\left[\bar{N}_*\left(s,z_j\right)+\bar{N}_*\left(s,z_{j+1}\right)\right]\left[\bar{\varepsilon}_z^{(G)}\left(s,z_{j+1},z_i\right)-\bar{\varepsilon}_z^{(G)}\left(s,z_j,z_i\right)\right]$$

$$=s\,\bar{Q}(s)\bar{\varepsilon}_z^{(G)}(s,0,z_i),\ i=1\sim N_p. \tag{4.18}$$

By solving equation (4.18), N_p discrete transformed axial forces of the fictitious pile can be obtained numerically. As mentioned earlier, once the axial forces for the fictitious pile are obtained, the axial force $\bar{N}(s,z)$ of the pile, the vertical displacements $\bar{u}_z(s,z)$ and the pile-side pore pressure $\bar{p}(s,z)$ of the layered TISS in the transformed domain can all be determined numerically using their respective following equations.

$$\bar{N}(s,z_i) = -s\bar{Q}(s)\,\bar{f}_z^{(G)}(s,0,z_i) +$$

$$\frac{1}{2}\sum_{j=1}^{N_d} s\left[\bar{N}_*\left(s,z_j\right)+\bar{N}_*\left(s,z_{j+1}\right)\right]\left[\bar{f}_z^{(G)}\left(s,z_{j+1},z_i\right)-\bar{f}_z^{(G)}\left(s,z_j,z_i\right)\right],\ i=1\sim N_p; \quad (4.19)$$

$$\bar{u}_z(s,z_i) = s\bar{Q}(s)\bar{u}_z^{(G)}(s,0,z_i) -$$

$$\frac{1}{2}\sum_{j=1}^{N_d} s\left[\bar{N}_*\left(s,z_j\right)+\bar{N}_*\left(s,z_{j+1}\right)\right]\left[\bar{u}_z^{(G)}\left(s,z_{j+1},z_i\right)-\bar{u}_z^{(G)}\left(s,z_j,z_i\right)\right],\ i=1\sim N_p; \quad (4.20)$$

$$\bar{p}(s,z_i) = s\bar{Q}(s)\,\bar{p}^{(G)}(s,0,z_i) -$$

$$\frac{1}{2}\sum_{j=1}^{N_d} s\left[\bar{N}_*\left(s,z_j\right)+\bar{N}_*\left(s,z_{j+1}\right)\right]\left[\bar{p}^{(G)}\left(s,z_{j+1},z_i\right)-\bar{p}^{(G)}\left(s,z_j,z_i\right)\right],\ i=1\sim N_p. \quad (4.21)$$

Similarly, solving the above equations (4.19)~(4.21), N_p discrete transformed axial forces of the pile, vertical displacements and the pile-side pore pressure of the layered TISS can be numerically obtained, respectively.

Note that the obtained solution for the pile is in the transformed domain. In order to retrieve the solution in the time domain, an inversion of the Hankel-Laplace transform (Chapter 2) has to be performed numerically. First, the inversion of the Hankel transform involves evaluation of an infinite integral as shown in equation (2.2). Here, evaluation of the infinite integral associated with the inverse Hankel transform is accomplished by numerical integration, which is performed by calling the subroutine DQDAGI in IMSL. For the numerical examples presented in this study, a relatively small error can be achieved. Second, as mentioned earlier, in this study, the inversion of the Laplace transform is accomplished by using the Schapery's method. According to the Schapery's method [51], the function in the time domain can be retrieved by the corresponding function in the Laplace transformed domain via the following formula:

$$f(t) = [s\bar{f}(s)]_{s=1/2t}, \tag{4.22}$$

where $f(t)$ and $\bar{f}(s)$ represent the function in the time domain and Laplace transformed domain, respectively.

4.4 Summary

In this chapter, the Fredholm integral equations for the vertically loaded pile embedded in the layered TISS was developed with the basis of the elementary solution for a layered TISS obtained in the previous chapter (**Chapter 3**), together with adopting the fictitious pile method due to Muki & Sternberg. First, the pile-soil system was decomposed into two parts, namely, the fictitious pile and the extended half-space and it was assumed that the axial strain of the fictitious pile is equal to the vertical strain of the extended layered TISS along the z axis. Then, based on the force acting on the layered TISS half-space together with the fundamental solution and the Laplace transform, the transformed second kind Fredholm integral equations for the axially loaded pile was established in which the unknown becomes the axial force of the fictitious pile. With the fictitious axial force obtained, other integral equations for pile axial force and other variables were developed in the Laplace transformed domain. This chapter also highlighted the numerical inversion methods of the Hankel-Laplace transformations adopted in this research. In the end, the numerical solution for the second kind of Fredholm integral equations was detailed, taking into account the number of interfaces present between the soil layers of the half-space.

Chapter 5 Numerical results and corresponding analyses

In this section, numerical results for the response of the layered TISS to a point vertical force and the vertically loaded pile embedded in a layered TISS obtained by the proposed model are presented. First, numerical analysis on the behavior of the layered TISS is presented. Then, to validate the proposed integral equation model for the pile, results of this paper are compared with those of two existing solutions. Later, a parametric study on the effect of different parameters on the behavior the pile in a layered TISS is carried out.

For the convenience of presentation, the following non-dimensional quantities are defined:

$$z^* = \frac{z}{L_R},\ R^* = \frac{r}{L_R},\ t^* = \frac{k_R t}{L_R},\ u^* = \frac{u_z(z)}{L_R},\ v^* = \frac{u_z^{(G)}(z)}{L_R},\ w^* = \frac{u_r^{(G)}(z)}{L_R}$$

$$N* = \frac{N(z)}{\mu_R L_R^2},\ s^* = \frac{\sigma_{zz}^{(G)}(z)}{\mu_R L_R^2},\ p^* = \frac{p(z)}{\mu_R},\ p^{**} = \frac{p^{(G)}(z)}{\mu_R}\ \ Q^* = \frac{Q}{\mu_R L_R^2}, \tag{5.1}$$

in which L_R, μ_R and k_R are referred to as the reference length, shear modulus, and coefficient of permeability; the quantities z^*, R^*, u^*, N^*, p^*, t^* and Q^* represent the dimensionless depth, radius, displacement, pile axial force, pore pressure, time, and the applied force, respectively. While, the quantities v^*, w^*, s^*, p^{**} denote the dimensionless fundamental solution for the vertical displacement, horizontal displacement, vertical stress and the soil pore pressure in the time domain, respectively.

5.1 Numerical analysis for a layered TISS subjected to a point force

In this section, with the aid of an example, the response of a three-layered TISS to a vertical point force buried in the layered TISS is calculated by the proposed RTM method.

γ_w

Numerical results are given to discuss the effect of the transverse isotropy property of the soil.

In this example, the half-space TISS is assumed to consist of three layers, namely, two overlying soil layers and an underlying half-space layer. The material parameters for the three soil layers are given in Table 5.1. In order to investigate the influence of the stiffness ratio ($\eta = E_h / E_v$) on the response of the half-space TISS, three different cases, each associated with a different stiffness ratio value are considered. A stiffness ratio of $\eta = 0.5$ is used for Case 1; $\eta = 1.5$ for Case 2 ; and $\eta = 3$ Case 3. The vertical downward point force is applied at a depth of $z_s = 6$ m, and the depths of the two receiver points are $z_{p1} = 3$ m and $z_{p2} = 9$ m. The radii of the two receiver points are $R_{p1} = R_{p2} = 3$ m. In this section, the thickness, shear modulus μ_v and coefficient of vertical permeability k_v of the first soil layer are used as the reference length L_R, shear modulus μ_R, and coefficient of permeability k_R, respectively.

Table 5. 1 Parameters for the soil used in the example (sect. 5.1)

Layer number	h / m	E_v / Pa	μ_v / Pa	k_v, k_h / m·s^{-1}	ν_h	ν_{hv}	γ_w / N·m^{-3}
1	8	2.8×10^6	1.0×10^6	1.0×10^{-7}	0.4	0.4	9.8×10^3
2	8	2.8×10^7	1.0×10^7	1.0×10^{-7}	0.4	0.4	9.8×10^3
3	-	2.8×10^8	1.0×10^8	1.0×10^{-7}	0.4	0.4	9.8×10^3

The following Figure 5.1 depicts the time-dependent variation of the non-dimensional vertical displacement v^*, the non-dimensional horizontal displacement w^*, the non-dimensional vertical stress s^* and the non-dimensional pore pressure p^{**} at the two receiver points of the layered saturated soil caused by the non-dimensional unit vertical point force.

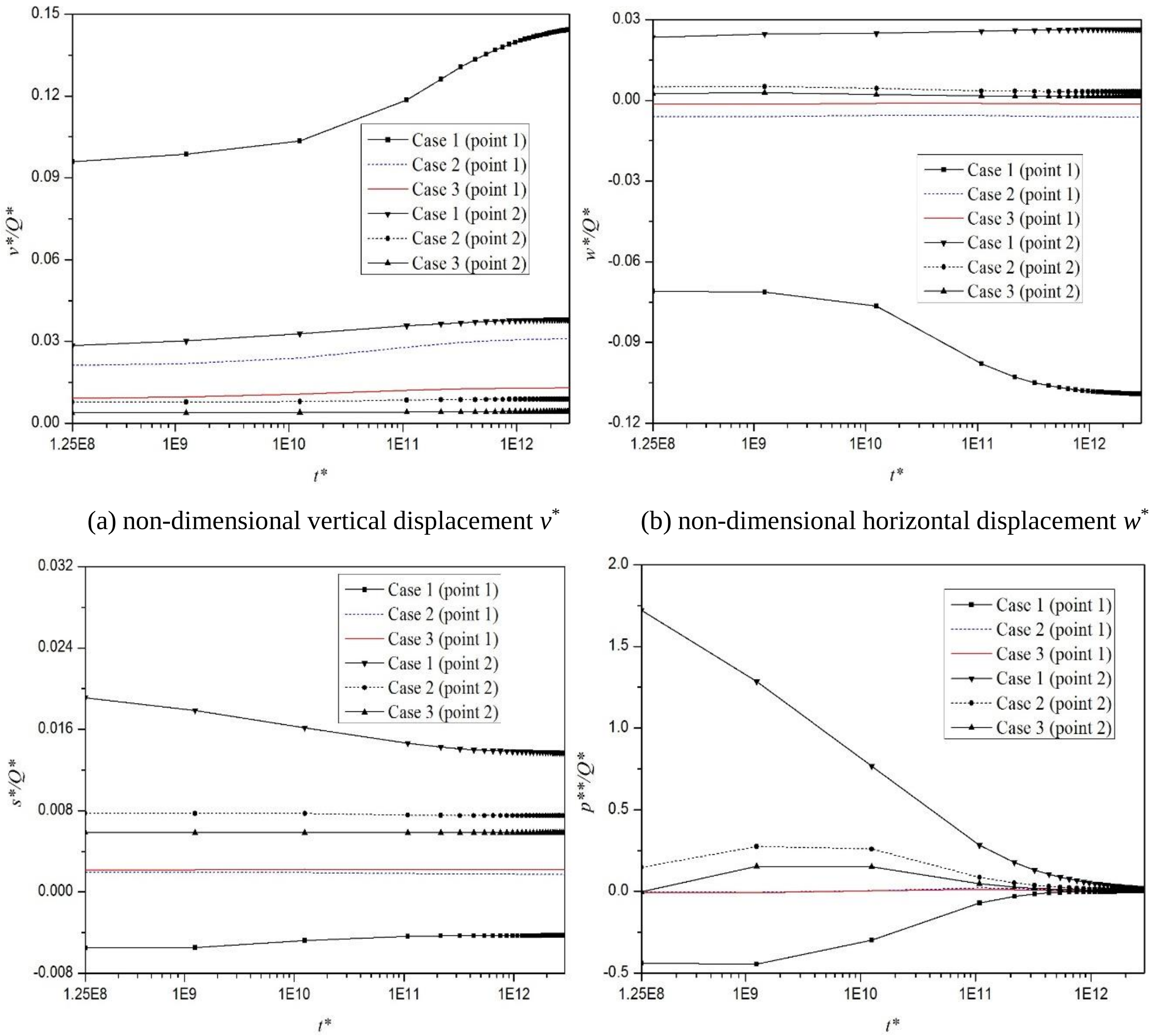

(a) non-dimensional vertical displacement v^* (b) non-dimensional horizontal displacement w^*

(c) non-dimensional vertical stress s^* (d) non-dimensional pore pressure p^{**}

Figure 5. 1 Behavior of the two receiver points of the layered saturated soil due to non-dimensional unit vertical point force (a) non-dimensional vertical displacement v^*; (b) non-dimensional horizontal displacement w^*; (c) non-dimensional stress s^*; (d) non-dimensional soil pore pressure p^{**}

It follows in Figure 5.1 (a) that in all the two cases, the vertical displacement at all the two receiver points increases over time. The vertical displacement will decrease with the increase of the stiffness ratio at both receivers. it also shown that comparing the curves at both receiver points, the vertical displacement decreases as the depth increases. Figure 5.1 (b) illustrates that for all case, the horizontal displacement at point one is negative, while positive at point two. It can be seen that except point one in Case 1, all other curves are consistent with each other with a slight increase over time. Unlike the vertical displacement, the horizontal displacement increases with the increase of depth. At the first receiver (point one), the horizontal displacement increases with stiffness ratio, while decreasing at point two. Figure 5.1 (a) and (b) also proves that, as the stiffness ratio increases, the difference between the displacements curves at the two points will tend to get smaller.

Figure 5.1 (c) shows that the vertical stress slightly increases with the increase of the time except that at point 2 for Case 1. At the first receiver point one, the vertical stress increases with the stiffness ratio, while it becomes opposite at the second receiver point two. Figure 5.1 (c) also shows a tensile stress at point one and like the vertical and horizontal displacement, the difference between the vertical stresses at both points reduces as the stiffness ratio increases. The pore pressure as depicted in Figure 5.1 (d), tends to zero as the time increases due to the consolidation process. However, in the beginning, a negative pore pressure is observed at the first receiver point one and a positive at point two. It is also shown that the pore pressure at the second receiver (point 2) will increase with a stiffness ratio while decreasing at point one.

5.2 Validation of the proposed integral equation model for the pile

Niumpradit & Karasudhi [20] obtained the final solution for the axial force of the axially loaded pile embedded in the isotropic poroelastic half-space. To compare our results with the final solution of [20], in the present study, the time takes a large value and the relevant parameters are set as the pile length-diameter ratio $L/d = 20$; the soil Poisson's ratio $v_h = v_{hv} = v_{vh} = 0.25$ and $\eta = E_h / E_v = 1$, where E_h and E_v are the soil's horizontal and vertical Young's moduli. As depicted in Figure 5.2, the pile axial forces corresponding to the above parameters and different pile-soil Young's modulus ratio (E_p / E_v) obtained by the proposed model in this study agree with those obtained by Niumpradit & Karasudhi [20], thus, validating the proposed model.

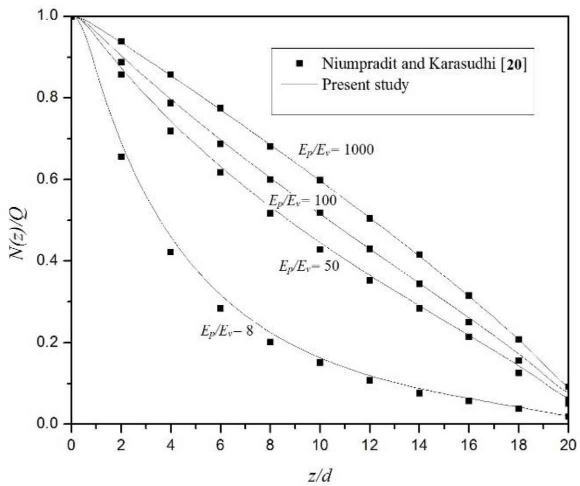

Figure 5. 2 Comparison of the pile axial force along the depth obtained in the present study with those by Niumpradit & Karasudhi [20]

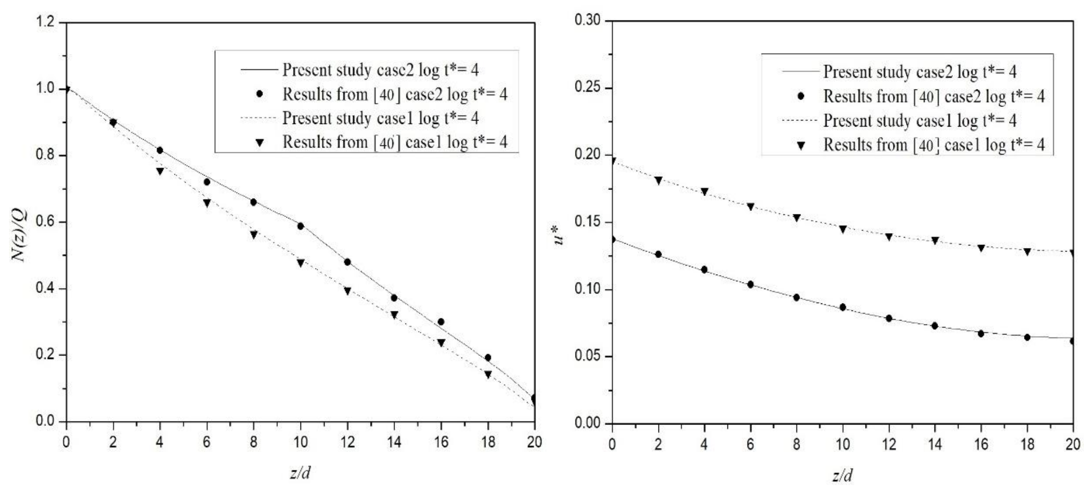

(a) the pile axial force *N(z)/Q* (b) the vertical displacement u^*

Figure 5. 3 Comparison of the results obtained in the present study with those by Ai et al. [40] (a) the pile axial force due to a unit point load *N(z)/Q*; (b) the non-dimensional vertical displacement u^*

Ai et al. [40] investigated the influence of the stratification of the soil on the response of the pile at different times. Two different cases, namely, Case 1 corresponding to a single layer half-space and Case 2 a stratified soil consisting of three isotropic layers with the shear moduli ratio equal to $\mu_{v1}:\mu_{v2}:\mu_{v3}=1:2:3$ are considered in their research, wherein the subscripts 1, 2 and 3 represent the first layer, second layer, and third layer, respectively. Other parameters for the pile-soil system are as follows: the pile length-diameter ratio $L/d=20$; the soil Poisson's ratio $v_h=v_{hv}=v_{vh}=0.3$; the pile-soil Young's modulus ratio $E_p/E_v=300$; the coefficient of permeability $k_h=k_v=1.2\times10^{-6}$ ms^{-1}; the soil layer's thicknesses for the second case are $h_1/d=h_2/d=10$; the soil stiffness ratio is $\eta=E_h/E_v=1$. In this example, the non-dimensional vertical displacement and time are defined as $u^*=u(z)AE_R/QR$ and $t^*=2k_R\mu_R t/\gamma_w R^2$, in which the reference E_R, μ_R, and k_R are taken as the vertical Young's modulus, the shear modulus and the coefficient of vertical permeability of the first layer, respectively; $\gamma_w=9.8\times10^3$ Nm^{-3}. Figures 5.3 (a) and (b) show clearly that the pile axial force and the dimensionless vertical displacement obtained by the proposed model agree with those obtained by Ai et al. [40] for a vertically loaded pile in a multilayered saturated soil perfectly, again validating the proposed model.

5.3 Influence of the soil transverse isotropy property (η)

In this section, one numerical example is used to present the effect of the ratio of the soil horizontal Young's modulus to the vertical Young's modulus (the stiffness ratio $\eta=E_h/E_v$) on the response of the vertically loaded pile embedded in the three-layered half-space TISS. Four different stiffness ratios, i.e., $\eta=0.5$, $\eta=1.5$, $\eta=2$ and $\eta=3$ are chosen for Case 1, Case 2, Case 3 and Case 4, respectively, to display how the variation of the horizontal Young's modulus with respect to the vertical Young's moduli of the three layers affects the pile axial force, the displacement and the soil pore pressure on the pile side. In this example, for each stiffness ratio η, a stratified soil consisting of two overlying soil layers and one underlying half-space layer defined by their shear moduli ratio: $\mu_{v1}:\mu_{v2}:\mu_{v3}=1:1:2$, is associated. The values of soil parameters in all the four cases are tabulated in Table 5.2 and the pile parameters are as follows: length $L=20$ m, radius $R=0.25$ m, and the Young's modulus $E_p=2.6\times10^9$ Pa. Since the proposed model is time-dependent, the results after 1 day ($t=8.64\times10^4$ s) and 30 days ($t=2.592\times10^6$ s) are discussed in this example. In this section, the thickness, shear modulus μ_v and coefficient of vertical permeability k_v of the first soil layer are used as the reference length L_R, shear modulus μ_R, and coefficient of permeability k_R, respectively.

Table 5. 2 Parameters for the soil used in the example (sect. 5.3)

Layer number	h / m	E_v / Pa	μ_v / Pa	k_v, k_h / $\mathrm{m\cdot s^{-1}}$	ν_h	ν_{hv}	γ_w / $\mathrm{N\cdot m^{-3}}$
1	10	2.6×10^7	1.0×10^7	1.2×10^{-7}	0.3	0.3	9.8×10^3
2	10	2.6×10^7	1.0×10^7	1.2×10^{-7}	0.3	0.3	9.8×10^3
3	-	5.2×10^7	2.0×10^7	1.2×10^{-7}	0.3	0.3	9.8×10^3

The variation curves of the normalized pile axial force N^*, vertical displacement u^* and the pore pressure p^* versus the normalized depth are plotted in Figure 5.4-5.6, respectively. And a comparison of all the four cases shows a great impact of the soil stiffness ratio on the pile response.

As expected, the results shown in Figure 5.4 illustrate that the pile axial force will increase as the stiffness ratio decreases except at the pile top and bottom where the curves seem to converge.

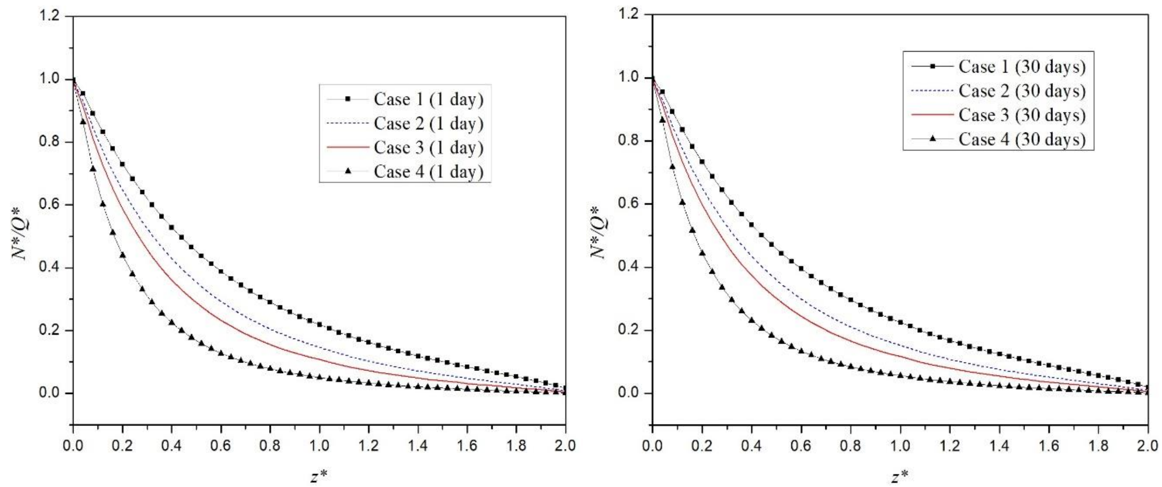

(a) 1 Day (b) 30 Days

Figure 5. 4 Variation of the non-dimensional pile axial force N^* along the depth at the times of (a) 1 Day; (b) 30 Days

It is also shown in both Figure 5.4 (a) and (b) that for all Cases, the pile axial force decreases with the increase of the depth, while the former will increase as time increases.

Similarly, Figure 5.5 illustrates that the vertical displacement of the pile also decreases as the depth increases. Fig 5.5 also shows that unlike the axial force, a larger stiffness ratio corresponds to a larger vertical displacement of the pile. It can be seen in both Figure 5.4 and 5.5 that the decrement of both the pile axial force and vertical displacement along the first layer of the saturated half-space is bigger than that along the middle layer.

As depicted in Figure 5.6, the pore pressure on the pile-side tends to zero as the time increases. For all three Cases, the pore pressure at the top of the pile vanishes, since the top of the half-space soil is assumed to be permeable. All the curves first increase, then after their corresponding marked peak, they decrease with the depth. Figure 5.6 also illustrates that the pore pressure increases with the increase of the stiffness ratio. However, in Figure 5.6 (b), both curves in Case 3 and Case 4 intersect at one point in the first layer.

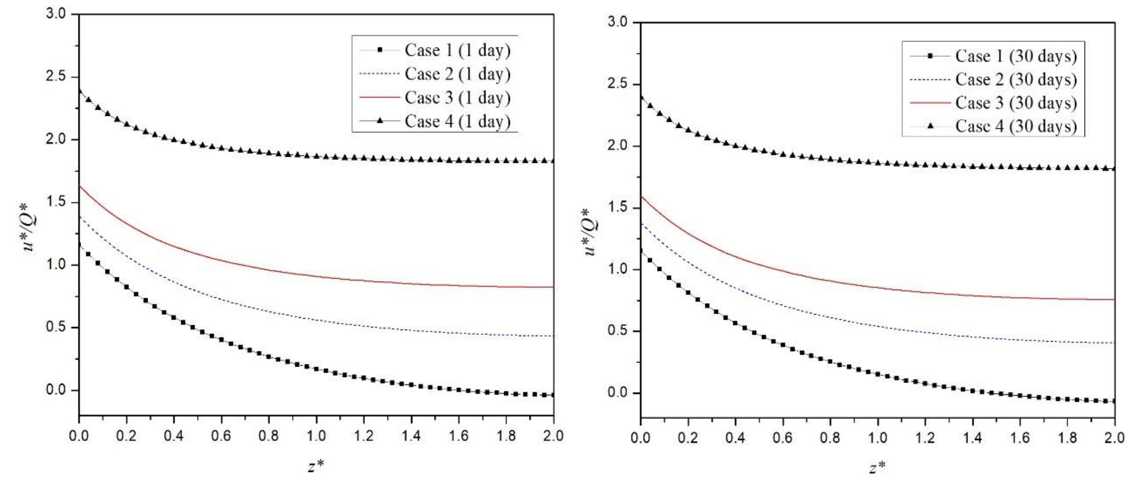

(a) 1 Day (b) 30 Days

Figure 5. 5 Variation of the non-dimensional pile vertical displacement u^* along the depth at the times of (a) 1 Day; (b) 30 Days

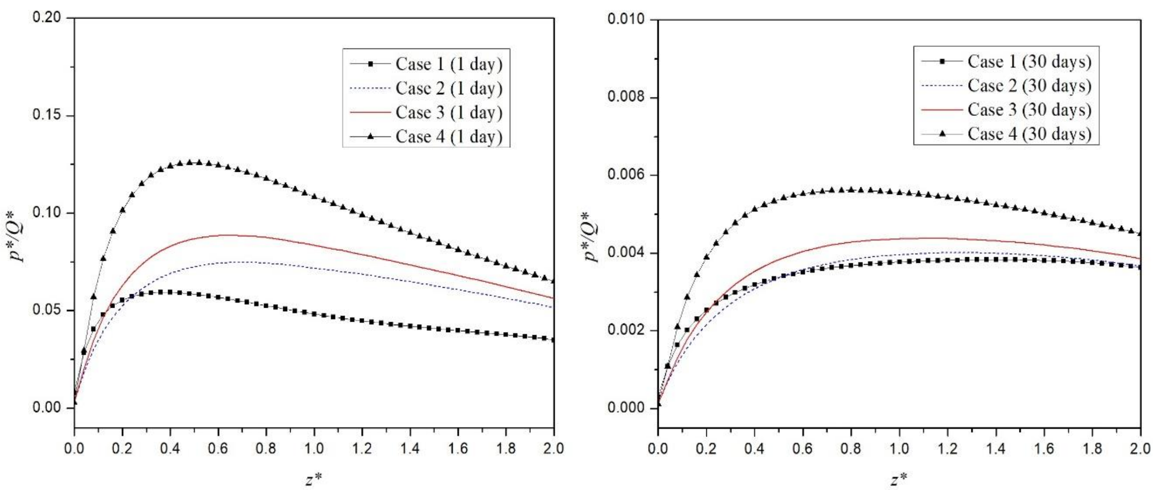

(a) 1 Day (b) 30 Days

Figure 5. 6 Variation of the non-dimensional pore pressure p^* at the pile side along the depth at the times of (a) 1 Day; (b) 30 Days

5.4 Influence of a stratified soil on the pile response

In order to analyze the influence of the stratified character of the medium on the behavior of a vertically loaded pile, two parametric examples each associated with a different pile length L are performed in this section to present the non-dimensional pile axial force, the non-dimensional vertical displacement and the non-dimensional soil pore pressure at two different times, i.e., $t = 8.64 \times 10^4$ s (one day) and $t = 2.592 \times 10^6$ s (thirty days). Similarly, in these two examples, a three-layered soil is chosen and four different cases associated with the variation of the three layer's moduli are considered: Case 1 denotes a three-layered TISS with a harder middle layer in which the layers shear moduli ratio is given as: $\mu_{v1}:\mu_{v2}:\mu_{v3}=1:2:1$; Case 2 symbolizes a three-layered TISS with a softer middle layer with the shear moduli ratio defined as: $\mu_{v1}:\mu_{v2}:\mu_{v3}=1:1/2:1$; Case 3 corresponds to a homogeneous half-space TISS; and Case 4 a three-layered TISS with the modulus that increases with the depth, i.e., $\mu_{v1}:\mu_{v2}:\mu_{v3}=1:2:3$. The stiffness ratio $\eta=2$ is held constant in both examples and for every layer, a new parameter $m=\mu_v/E_v=0.4$ is defined as the ratio of the shear modulus to the vertical Young's modulus. Moreover, the values of the soil parameters for this section are given in Table 5.2, while the pile parameters are given as the length $L=15$ m in the first example and $L=25$ m for the second example; the radius and the pile Young's modulus are kept constant in both examples as $R=0.25$ m and $E_p=5\times10^9$, respectively. Likewise, in this section, the thickness, shear modulus μ_v and coefficient of vertical permeability k_v of the first soil layer are used as the reference length L_R, shear modulus μ_R, and coefficient of permeability k_R, respectively.

Table 5. 3 Parameters for the soil used in the example (sect. 5.4)

Layer number	h / m	μ_v / Pa				ν_h	ν_{hv}	γ_w / N·m^{-3}	k_v,k_h / m·s^{-1}
		Case 1	Case 2	Case 3	Case 4				
1	10	1.0×10^7	1.0×10^7	1.0×10^7	1.0×10^7	0.25	0.25	9.8×10^3	1.2×10^{-7}
2	10	2.0×10^7	0.5×10^7	1.0×10^7	2.0×10^7	0.25	0.25	9.8×10^3	1.2×10^{-7}
3	-	1.0×10^7	1.0×10^7	1.0×10^7	3.0×10^7	0.25	0.25	9.8×10^3	1.2×10^{-7}

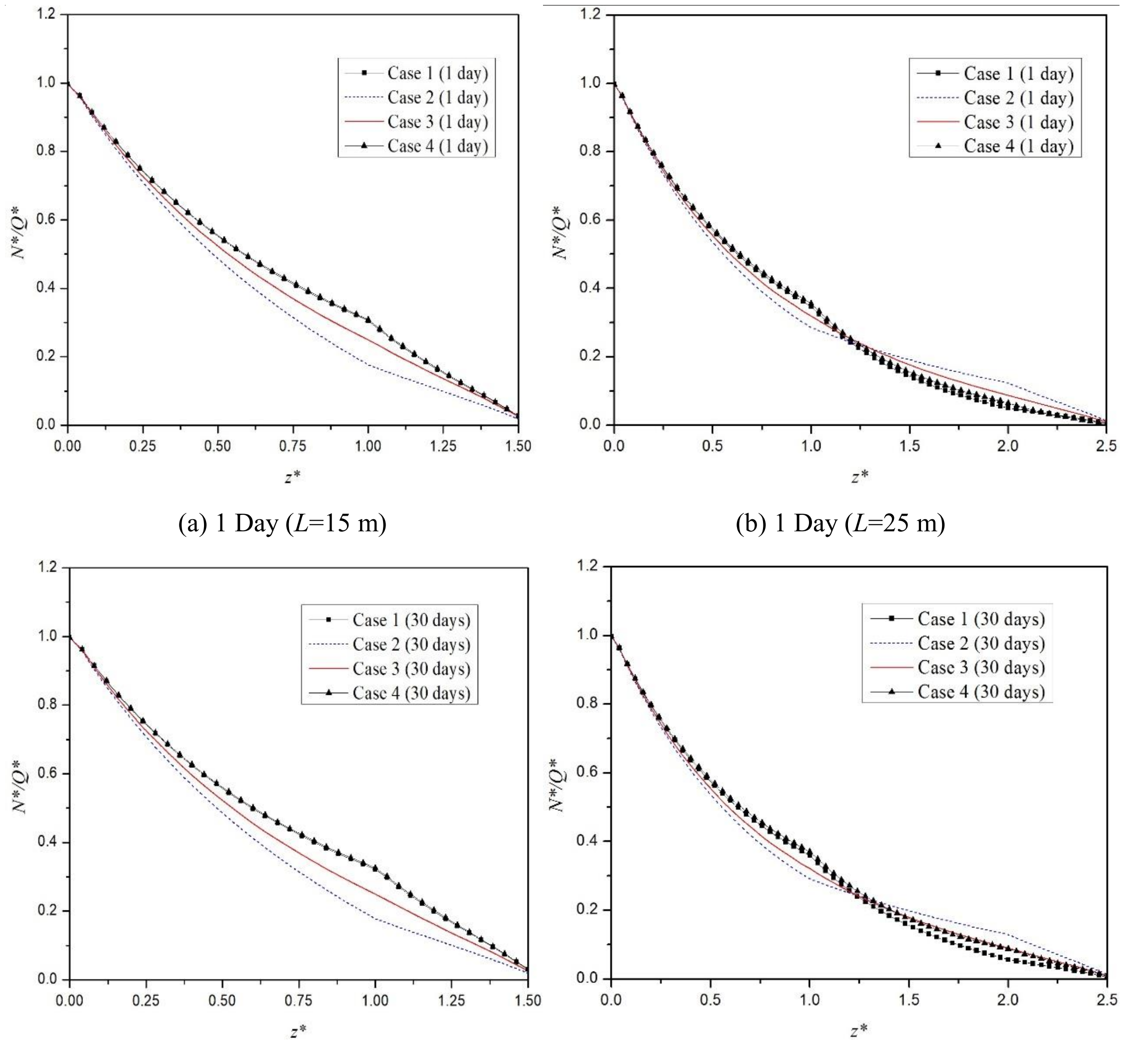

(a) 1 Day (L=15 m) (b) 1 Day (L=25 m)

(c) 30 Days (L=15 m) (d) 30 Days (L=25 m)

Figure 5. 7 Variation of the non-dimensional pile axial force N^* along the depth at the times of (a) 1 Day (L=15 m); (b) 1 Day (L=25 m); (c) 30 Days (L=15 m); (d) 30 Days (L=25 m)

The character of a stratified saturated soil as shown in Figures 5.7-5.9 has a meaningful impact on the response of a circular pile loaded vertically on top. Figures 5.7 (a) and (c) show that at the pile top, the axial force curves in all cases coincide, but as the depth increases, the pile axial force in the case of the half-space with a soft middle layer (Case 2) will be comparatively smaller and larger in both Case 1 and Case 4. As mentioned earlier, the soil properties in case 1 and case 4 are similar for the first and second layer, which explain why both curves in Case 1 and Case 4 overlap each other. It is noted, however, as the depth increases with the presence of a longer pile (L=25 m) as shown in Figure 5.7 (b) and (d), the axial force in Case 1 will tend to be smaller compared to that in case 4 and the axial force in Case 2 will this time be larger compared to those in other cases at the same depth. It is also noted that the axial force at the bottom of the pile in all cases approaches zero or a small value.

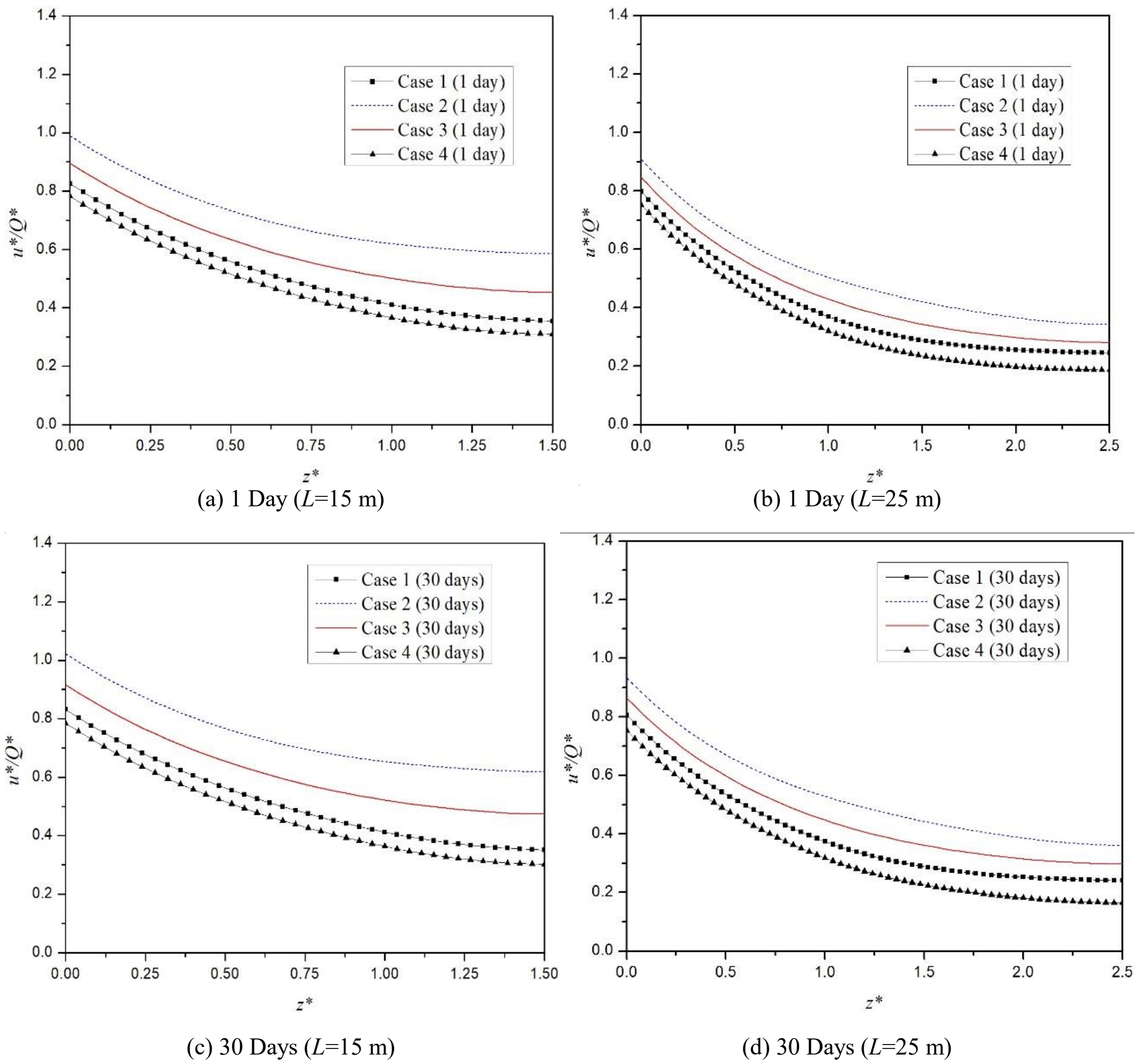

(a) 1 Day (L=15 m) (b) 1 Day (L=25 m)

(c) 30 Days (L=15 m) (d) 30 Days (L=25 m)

Figure 5. 8 Variation of the non-dimensional pile vertical displacement u^* along the depth at the times of (a) 1 Day (L=15 m); (b) 1 Day (L=25 m); (c) 30 Days (L=15 m); (d) 30 Days (L=25 m)

As for the pile vertical displacement, Figure 5.8 illustrates that the displacement in all cases is consistent with each other. It can also be seen that Case 4 in which the half-space has three layers with incremental shear modulus, presents a smaller vertical displacement compared to other cases at the same depth. A larger displacement occurs in case 2. The soil pore pressure on the pile-side in the second and third layer of the half space as shown in Figure 5.9 (a) and (b) will be higher with the half-space that has a soft middle layer (Case 2) and smaller in the case of a hard middle layer. However, with the time increasing, the soil pore pressure will be smaller in Case 3 compared to those in other cases at the same depth.

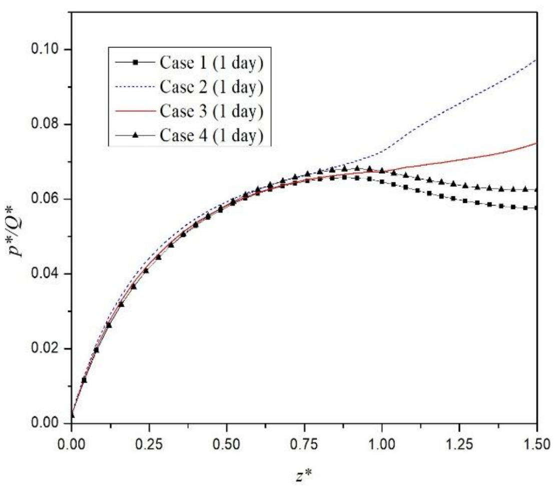

(a) 1 Day (L=15 m)

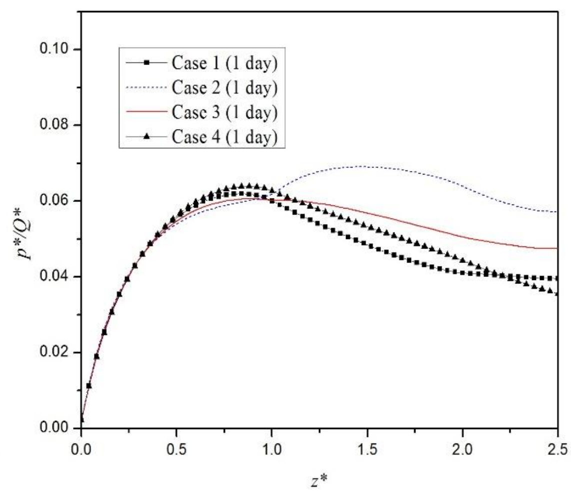

(b) 1 Day (L=25 m)

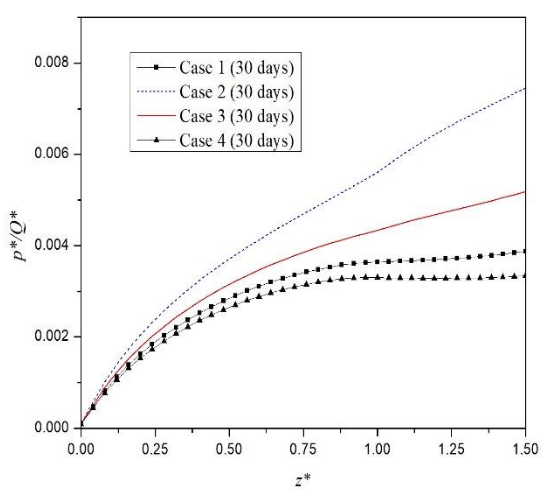

(c) 30 Days (L=15 m)

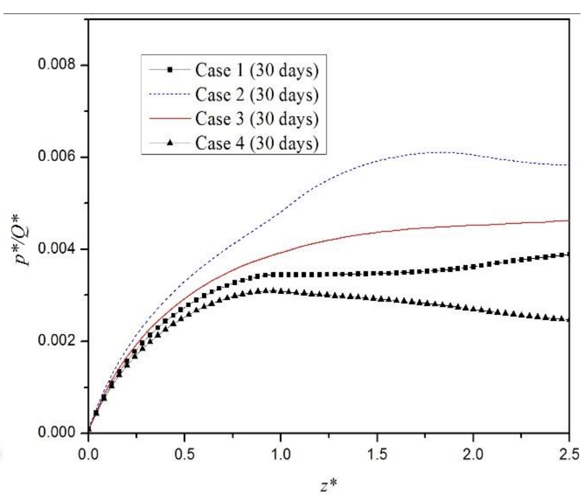

(d) 30 Days (L=25 m)

Figure 5. 9 Variation of the non-dimensional pore pressure p^* at the pile side along the depth at the times of (a) 1 Day (L=15 m); (b) 1 Day (L=25 m); (c) 30 Days (L=15 m); (d) 30 Days (L=25 m)

From Figures 5.7 and 5.8, it can be seen that the pile axial force and vertical displacement decrease with the increase of the depth and increase over time. On the other hand, the soil pore pressure decreases to a small value as the time increases as shown in Fig 5.9. This indicates the final stage of the consolidation as the pore pressure dissipates completely. Along the depth, the pore pressure increases first, then decrease.

In this section, with two different examples mentioned earlier, the influence of the pile length was investigated, the results are shown in Figures 5.7-5.9. the results show that the pile vertical displacement and soil pore pressure decreases with the increase of the pile length, while the pile axial force increases for a longer pile.

5.5 Effect of the permeability of the middle layer

In this section, the influence of the permeability on the behavior of the pile embedded in a three-layered half-space TISS is investigated. Note that the half-space TISS is also composed of two overlying layers and one underlying layer, i.e., the underlying half-space. Three cases are considered in this section. For Case 1, all three layers have equal permeability; Case 2 corresponds to a high permeable middle layer; Case 3 to a less permeable middle layer. The parameters for the pile used in this section are set as length $L = 20$ m, radius $R = 0.3$ m, and the Young's modulus $E_p = 2.5\times10^9$ Pa, while the parameters for the soil are shown in Table 5.3. Similarly, the thickness, shear modulus μ_v and coefficient of vertical permeability k_v of the first soil layer are used as the reference length L_R, shear modulus μ_R, and coefficient of permeability k_R, respectively.

Figures 5.10 and 5.11 show that the influence of the permeability of the middle layer is almost negligible. It can also be seen that for all three cases, the vertical displacement increases as time increases. Moreover, both the axial force and vertical displacement decrease with the depth.

Table 5. 4 Parameters for the soil used in the example (sect. 5.5)

Layer number	h / m	k_v, k_h / $\mathrm{m \cdot s^{-1}}$			ν_h	ν_{hv}	γ_w / $\mathrm{N \cdot m^{-3}}$	E_h / Pa	E_v / Pa	μ_v / Pa
		Case 1	Case 2	Case 3						
1	10	1.0×10^{-8}	1.0×10^{-8}	1.0×10^{-8}	0.25	0.25	9.8×10^{3}	2.5×10^{7}	2.5×10^{7}	1.0×10^{7}
2	10	1.0×10^{-8}	1.0×10^{-7}	1.0×10^{-9}	0.25	0.25	9.8×10^{3}	2.5×10^{7}	2.5×10^{7}	1.0×10^{7}
3	-	1.0×10^{-8}	1.0×10^{-8}	1.0×10^{-8}	0.25	0.25	9.8×10^{3}	2.5×10^{7}	2.5×10^{7}	1.0×10^{7}

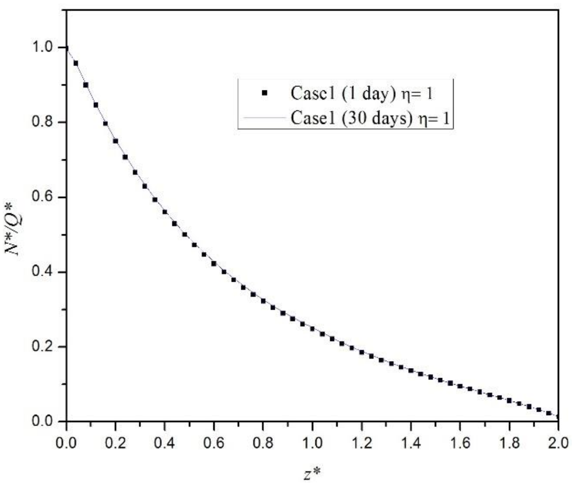

(a) N^* for Case 1

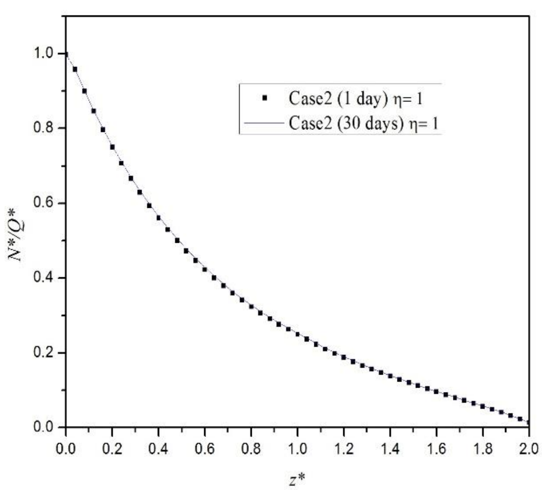

(b) N^* for Case 2

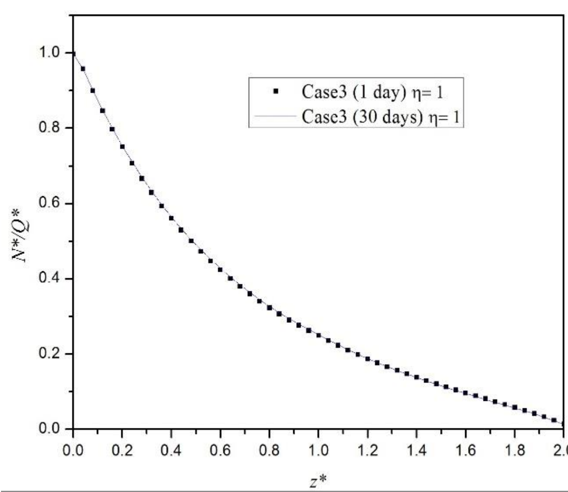

(c) N^* for Case 3

Figure 5. 10 Variation of the non-dimensional pile axial force N^* along the depth at the times of 1 Day and 30 Days: (a) N^* for Case 1; (b) N^* for Case 2; (c) N^* for Case 3

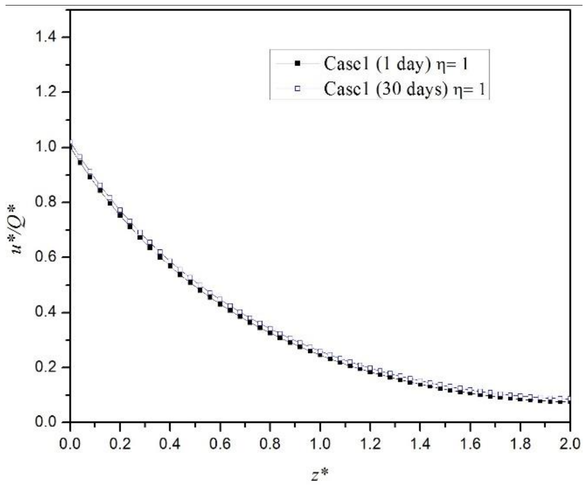

(a) u^* for Case 1

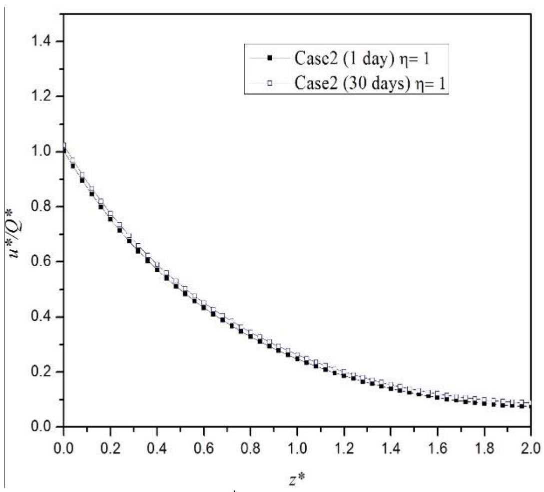

(b) u^* for Case 2

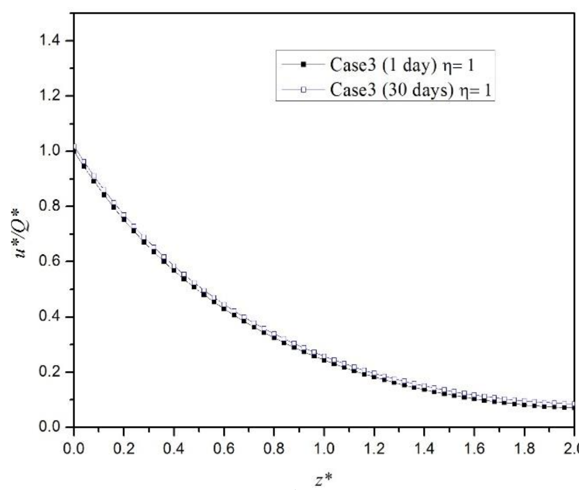

(c) u^* for Case 3

Figure 5. 11 Variation of the non-dimensional pile vertical displacement u^*along the depth at the times of 1 Day and 30 Days: (a) u^* for Case 1; (b) u^* for Case 2; (c) u^* for Case 3

Besides, as illustrated in Figure 5.12, the permeability of the middle layer has a significant influence on the pore pressure. The pore pressure is the largest when the half-space's middle layer is less permeable, i.e., Case 3, and smallest when the middle layer is highly permeable. The pore pressure at 30 days is much smaller than that at one day, which indicates that the pore pressure will dissipate with time for all three cases. Figure 5.12 (a) shows that at the time of one day, the variation of the pore pressure for the three cases is similar: it first increases with the depth; then, it achieves a peak value at a certain depth in the first layer; lastly, it will decrease with the depth.

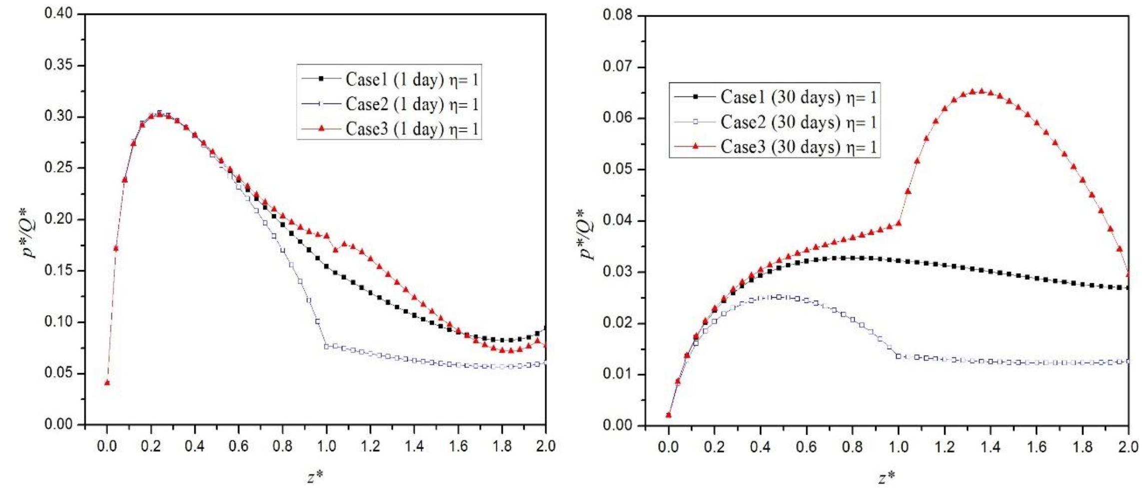

(a) 1 Day (b) 30 Days

Figure 5. 12 Variation of the non-dimensional pore pressure p^* at the pile side along the depth at the times of (a) 1 Day; (b) 30 Days

5.6 Summary

In this chapter, adopting the numerical solution methods (**Chapter** 2) and the solutions derived in **Chapter 3** and **Chapter 4** for the layered TISS half-space and the pile, respectively, parametric results were compiled and analyzed by means of the Fortran software and a discussion were made. It was also demonstrated that the proposed model for the integral equation for the pile comes into agreement with existing solutions. With different parametric examples, it was shown that different soil properties such as stratification, transverse isotropy, etc.., present a great impact on the time-dependent response of both the layered TISS subjected to a vertical unit point force and the vertically loaded pile embedded in a layered TISS.

Chapter 6 General conclusions and prospects

In this research, based on the fundamental solution, the integral equation method is used to develop a stable and efficient model that predicts the time-dependent response of a vertically loaded pile embedded in a layered TISS. The fundamental solution for the half-space TISS is obtained via the RTM method. Numerical results were compiled with the use of Fortran program. Based on the research conducted in this study, the following notes can be drawn:

(1) Results obtained by the proposed model developed in this paper are compared with those of existing solutions and a good agreement between the two solutions is observed. Thus, validating the proposed integral equation of the pile.

(2) The proposed RTM model shows that the ratio of the soil horizontal Young's modulus to the vertical Young's modulus significantly affects the response of the layered TISS subjected to a point vertical force. The vertical displacement is shown to decrease as the stiffness ratio increases, while a different scenario occurs depending on the depth of the receiver point for the vertical stress and horizontal displacement. In addition, with the increase of the stiffness ratio, the difference between two different points with the same radius in the layered TISS will tend to be small compared to that with a small stiffness ratio. The pore pressure will tend to dissipate in the soil at any depth due to the consolidation process. Besides, the vertical displacement at all depth increases over time.

(3) The parametric study presented in this paper also displays that the transverse isotropy property of the soil has a considerable influence on the behavior of the vertically loaded pile embedded in the layered half-space TISS. In addition, the time dependency is

also of great importance in predicting the pile response. A larger stiffness ratio will lead to an increase of both the pile vertical displacement and the pile-side soil pore pressure. An opposite situation is observed for the pile axial force which unlike the vertical displacement and the pore pressure tends to decrease with the stiffness ratio increasing. Besides, it is also found that both the vertical displacement and the axial force of the pile decrease with the increase of the depth and increase over time. As expected, the pore pressure along the pile-side tends to zero as the time increases.

(4) The character of a stratified saturated soil together with the length of the pile as shown in this research have a meaningful impact on the response of a circular pile loaded vertically on top. The pile axial force in the case of the half-space with a soft middle layer will be comparatively smaller and larger for a case where the half-space consists of a hard middle layer. It is also noted that the axial force at the bottom of the pile in all cases approaches zero or a small value. The vertical displacement will be the smallest in the half-space that has three layers with incremental shear modulus and the largest in the case of a three-layered half-space with a soft middle layer. the results also show that the pile vertical displacement and soil pore pressure decreases with the increase of the pile length, while the pile axial force increases for a longer pile.

(5) The permeability of the middle layer of the three-layered half-space TISS soil has a considerable influence on the pore pressure along the pile-side. The pore pressure is larger when the middle layer is less permeable and smaller when the middle layer is highly permeable. Besides, due to the permeable assumption for the soil surface, the pore pressure tends to zero at the top of the pile.

(6) The proposed model provides a valuable tool for estimation of the response of a single pile embedded in a layered half-space TISS. In the further study, more practical engineering problems, such as the problem of the pile embedded in the layered TISS subjected to horizontal forces and the problem of pile groups in the layered TISS can be considered.

References

[1] Seed HB, Reese LC. The action of soft clay along friction piles [J]. American Society of Civil Engineers Transactions, 1955.

[2] Sowers GF, Martin C, Wilson LL, Fausold M. The bearing capacity of friction pile groups in homogeneous clay from model studies [C]. Proceedings of the Fifth International Conference on Soil Mechanics and Foundation Engineering, 1961.

[3] Coyle HM, Reese LC. Load transfer for axially loaded piles in clay [J]. Journal of the Soil Mechanics and Foundations Division, 1966; 92(2): 1-26.

[4] Poulos H. Analysis of the settlement of pile groups [J]. Geotechnique, 1968; 18(4): 449-71.

[5] Thurman A, D'Appolonia E. Computed movement of friction and end bearing piles embedded in uniform and stratified soils [C]. Proceedings of the Sixth International Conference on Soil Mechanics 2, 1965.

[6] Poulous H, Davis E. The settlement behavior of single axially loaded incompressible piles and piers [J]. Geotechnique, 1968; 18(4): 351-371.

[7] Poulos HG, Davis EH. Pile foundation analysis and design [M]. Wiley, NewYork, 1980.

[8] Mindlin RD. Force at a point in the interior of a semi-infinite solid [J]. Physics 1936; 7(5): 195-202.

[9] Poulos H, Mattes N. The behaviour of axially loaded end-bearing piles [J]. Géotechnique 1969; 19(2): 285-300.

[10] Butterfield R, Banerjee P. The elastic analysis of compressible piles and pile groups [J]. Geotechnique 1971; 21(1): 43-60.

[11] Muki R, Sternberg E. On the diffusion of an axial load from an infinite cylindrical bar embedded in an elastic medium [J]. International Journal of Solids and Structures 1969; 5(6): 587-605.

[12] Muki R, Sternberg E. Elastostatic load-transfer to a half-space from a partially embedded axially loaded rod [J]. International Journal of Solids and Structures 1970; 6(1): 69-90.

[13] Apirathvoraku V, Karasudhi P. Quasi-static bending of a cylindrical elastic bar partially embedded in a saturated elastic half-space [J]. International Journal of Solids and Structures 1980; 16(7): 625-44.

[14] Cao M, Chen L, Chen S. An innovative approach to evaluate the behaviour of vertically loaded pile groups based on elastic theory [J]. Journal of Lowland Technology International 2007; 9(1): 1-10.

[15] Selvadurai A, Rajapakse R. Axial stiffness of anchoring rods embedded in elastic media [J]. Canadian Journal of Civil Engineering 1990; 17(3): 321-328.

[16] Lu JF, Xu B, Wang J-H, Jeng D-S. Dynamic responses of a pile embedded in a layered poroelastic half-space to a harmonic axial loading [J]. Acta Mechanica 2009; 207(1-2): 29-49.

[17] Lu JF, Yin J, Shuai J. A model for predicting the frost-heave effect of a pile embedded in the frozen soil [J]. Cold Regions Science and Technology 2018; 146: 214-222.

[18] Rajapakse R, Shah A. On the longitudinal harmonic motion of an elastic bar embedded in an elastic half-space [J]. International Journal of Solids and Structures 1987; 23(2): 267-285.

[19] Pak RY, Saphores J-DM. On the response of a partially embedded rod to axial load [J]. Journal of Applied Mechanics 1991; 58(2): 599-602.

[20] Niumpradit B, Karasudhi P. Load transfer from an elastic pile to a saturated porous elastic soil [J]. International Journal for Numerical and Analytical Methods in Geomechanics 1981; 5(2): 115-138.

[21] Biot MA. General theory of three-dimensional consolidation [J]. Journal of Applied Physics 1941; 12(2): 155-164.

[22] Liang F, Song Z, Guo WD. Group interaction on vertically loaded piles in saturated poroelastic soil [J]. Computers and Geotechnics 2014; 56:1- 10.

[23] Banerjee P, Davies T. The behaviour of axially and laterally loaded single piles embedded in nonhomogeneous soils [J]. Geotechnique 1978; 28(3): 309-326.

[24] Davies T, Banerjee P. The displacement field due to a point load at the interface of a two layer elastic half-space [J]. Geotechnique 1978; 28(1): 43-56.

[25] Randolph MF, Wroth CP. Analysis of deformation of vertically loaded piles [J]. Journal of Geotechnical and Geoenvironmental Engineering 1978; 104(12): 1465-1488.

[26] Gibson R. Some results concerning displacements and stresses in a non-homogeneous elastic half-space [J]. Geotechnique 1967; 17(1): 58-67.

[27] Guo WD, Randolph MF. Vertically loaded piles in non-homogeneous media [J]. International Journal for Numerical and Analytical Methods in Geomechanics 1997; 21(8): 507-532.

[28] Poulos HG. Settlement of single piles in non homogeneous soil [J]. Journal of the Geotechnical Engineering Division 1979; 105(5): 627-642.

[29] Lee S, Kog Y, Karunaratne G. Axially loaded piles in layered soil [J]. Journal of Geotechnical Engineering 1987; 113(4): 366-381.

[30] Chin J, Chow Y, Poulos H. Numerical analysis of axially loaded vertical piles and pile groups [J]. Computers and Geotechnics 1990; 9(4): 273-290.

[31] Chan K, Karasudhi P, Lee S. Force at a point in the interior of a layered elastic half space [J]. International Journal of Solids and Structures 1974; 10(11): 1179-1199.

[32] Chow Y. Axially loaded piles and pile groups embedded in a cross-anisotropic soil [J]. Géotechnique 1989; 39(2): 203-212.

[33] Seo H, Prezzi M. Analytical solutions for a vertically loaded pile in multilayered soil [J]. Geomechanics and Geoengineering 2007; 2(1): 51-60.

[34] Lee C, Small J. Finite-layer analysis of axially loaded piles [J]. Journal of Geotechnical Engineering 1991; 117(11): 1706-1722.

[35] Almeida VS, de Paiva JB. Static analysis of soil/pile interaction in layered soil by BEM/BEM coupling [J]. Advances in Engineering Software 2007; 38(11-12): 835-845.

[36] Ai ZY, Yue Z. Elastic analysis of axially loaded single pile in multilayered soils [J]. International Journal of Engineering Science 2009; 47(11-12): 1079-1088.

[37] Lee K, Xiao Z. A new analytical model for settlement analysis of a single pile in multi-layered soil [J]. Soils and foundations 1999; 39(5): 131-143.

[38] Senjuntichai T, Sornpakdee N, Teerawong J, Rajapakse R. Time-dependent response of an axially loaded elastic bar in a multilayered poroelastic medium [J]. Journal of Engineering Mechanics 2007; 133(5): 578-587.

[39] Ai ZY, Cheng YC, Zeng WZ. Analytical layer-element solution to axisymmetric consolidation of multilayered soils [J]. Computers and Geotechnics 2011; 38(2): 227-232.

[40] Ai ZY, Wang LH, Hu YD. Load transfer from an axially loaded pile to multilayered saturated media [J]. Applied Mathematical Modelling 2016; 40(13-14): 6509-6522.

[41] Ai ZY, Li PC, Song X, Shi BK. Analysis of an axially loaded pile in saturated multi-layered soils with anisotropic permeability and elastic superstrata [J]. Computers and Geotechnics 2018; 98: 93-101.

[42] Barden L. Stresses and displacements in a cross-anisotropic soil [J]. Geotechnique 1963; 13(3): 198-210.

[43] Ai ZY, Wang Q. Transfer matrix solutions for axisymmetric consolidation of multilayered transversely isotropic soils [J]. Rock and Soil Mechanics 2009; 30(4): 921-925.

[44] Chen S, Chen L, Zhang L. The axisymmetric consolidation of a semi‐infinite transversely isotropic saturated soil. International Journal for Numerical and Analytical Methods in Geomechanics 2005; 29(13): 1249-1270.

[45] Ai ZY, Cheng YC. Analysis of vertically loaded piles in multilayered transversely isotropic soils by BEM [J]. Engineering Analysis with Boundary Elements 2013; 37(2): 327-335.

[46] Ai ZY, Chen YF, Jiang XB. Behavior of laterally and vertically loaded piles in multi-layered transversely isotropic soils [J]. Applied Mathematical Modelling 2017; 51: 561-573.

[47] Ai ZY, Feng DL, Cang NR. Analytical layer element solutions for deformations of transversely isotropic multilayered elastic media under nonaxisymmetric loading [J]. International Journal for Numerical and Analytical Methods in Geomechanics 2014 ;38(15): 1585-1599.

[48] Sneddon IN. The use of integral transforms. McGraw-Hill, New York, 1972.

[49] Durbin F. Numerical inversion of Laplace transforms: an efficient improvement to Dubner and Abate's method [J]. The Computer Journal, 1974; 17(4): 371-6.

[50] Stehfest H. Algorithm 368: Numerical inversion of Laplace transforms [D5] [J]. Communications of the ACM, 1970; 13(1): 47-49.

[51] Schapery R. Approximate Methods of Transform Inversion for Viscoelastic Stress Analysis [C]. Fourth US National Congress on Applied Mechanics, 1962.

[52] Lee E, Rogers TG. Solution of viscoelastic stress analysis problems using measured creep or relaxation functions [J]. Journal of Applied Mechanics 1963; 30(1): 127-133.

[53] Booker JR, Small J. Finite layer analysis of consolidation. I [J]. International Journal for Numerical and Analytical Methods in Geomechanics 1982; 6(2): 151-171.

[54] Booker J, Small J. Finite layer analysis of consolidation. II [J]. International Journal for Numerical and Analytical Methods in Geomechanics 1982; 6(2): 173-194.

[55] Mei GX, Yin JH, Zai JM, Yin ZZ, Ding XL, Zhu GF, et al. Consolidation analysis of a cross-anisotropic homogeneous elastic soil using a finite layer numerical method [J]. International Journal for Numerical and Analytical Methods in Geomechanics 2004; 28(2): 111-129.

[56] Christian JT, Boehmer JW. Plane strain consolidation by finite elements [J]. Journal of Soil Mechanics & Foundations Div, 1970; 96(4): 1435-1457.

[57] Sandhu RS, Wilson EL. Finite-element analysis of seepage in elastic media [J]. Journal of the Engineering Mechanics Division 1969; 95(3): 641-652.

[58] Cheng AHD, Liggett JA. Boundary integral equation method for linear porous-elasticity with applications to soil consolidation [J]. International Journal for Numerical Methods in Engineering 1984; 20(2): 255-278.

[59] Chiou YJ, Chi SY. Boundary element analysis of Biot consolidation in layered elastic soils. International Journal for Numerical and Analytical Methods in Geomechanics 1994; 18(6): 377-396.

[60] Chen G. Consolidation of multilayered half space with anisotropic permeability and compressible constituents [J]. International Journal of Solids and Structures 2004; 41(16-17): 4567-4586.

[61] Ai ZY, Cheng Z, Han J. State space solution to three-dimensional consolidation of multi-layered soils [J]. International Journal of Engineering Science 2008; 46(5): 486-498.

[62] Yue Z, Selvadurai A. Contact problem for saturated poroelastic solid [J]. Journal of Engineering Mechanics 1995; 121(4): 502-512.

[63] Pan E. Green's functions in layered poroelastic half-spaces [J]. International Journal for Numerical and Analytical Methods in Geomechanics 1999; 23(13): 1631-1653.

[64] Kennett B. Reflections, rays, and reverberations [J]. Bulletin of the Seismological Society of America 1974; 64(6): 1685-1696.

[65] Kennett B. Seismic wave propagation in stratified media [M]. Cambridge University Press , Cambridge, 1983.

[66] Xu B, Lu JF, Wang J-H. Dynamic response of a layered water-saturated half space to a moving load [J]. Computers and Geotechnics 2008; 35(1): 1-10.

[67] Lu JF, Shen RF, Shi MQ. Reflection–transmission matrix method for the consolidation of a multilayered saturated soil [J]. International Journal for Numerical and Analytical Methods in Geomechanics 2016; 40(11): 1594-1622.

Appendixes

I. The coefficient matrix

The coefficient matrix $\mathbf{A}(r,t)$ of the system of partial differential equations as shown in equation (3.13) is as follows:

$$\mathbf{A}(r,t)=\begin{bmatrix} \mathrm{B}_1 & \mathrm{B}_2 \\ \mathrm{B}_3 & \mathrm{B}_4 \end{bmatrix}, \tag{6.1}$$

with $\mathrm{B}_1=\begin{bmatrix} 0 & -a_2\left(\frac{\partial}{\partial r}+\frac{1}{r}\right) & 0 \\ -\frac{\partial}{\partial r} & 0 & 0 \\ 0 & -\frac{\partial}{\partial t}\left[(1-a_2)\left(\frac{\partial}{\partial r}+\frac{1}{r}\right)\right] & 0 \end{bmatrix}$, $\mathrm{B}_2=\begin{bmatrix} -a_3 & 0 & a_3 \\ 0 & -a_1 & 0 \\ a_3\frac{\partial}{\partial t} & 0 & -a_3\frac{\partial}{\partial t}+k_h'\left(\frac{\partial^2}{\partial r^2}+\frac{\partial}{r\partial r}\right) \end{bmatrix}$,

$\mathrm{B}_3=\begin{bmatrix} 0 & 0 & 0 \\ 0 & a_4\left(\frac{\partial^2}{\partial r^2}+\frac{\partial}{r\partial r}-\frac{1}{r^2}\right) & 0 \\ 0 & 0 & -\frac{1}{k_v'} \end{bmatrix}$, $\mathrm{B}_4=\begin{bmatrix} 0 & -\left(\frac{\partial}{\partial r}+\frac{1}{r}\right) & 0 \\ -a_2\frac{\partial}{\partial r} & 0 & (a_2-1)\frac{\partial}{\partial r} \\ 0 & 0 & 0 \end{bmatrix}$, in which

$a_1=1/c_{44}$, $a_2=c_{13}/c_{33}$, $a_1=1/c_{33}$, and $a_4=(c_{11}c_{33}-c_{13}^2)/c_{33}$.

II. Comments about the fundamental solutions of the layered TISS soil

As mentioned earlier, the fundamental solution of the axial force for the layered TISS fulfills the following relation:

$$f_z^{(G)}(t,z_+,z)-f_z^{(G)}(t,z_-,z)=-1. \tag{6.2}$$

The constitutive relation of the effective stress in the vertical direction $\sigma_{zz}'^{(G)}$ of the TISS in the cylindrical coordinate system given in equation (3.3) can also be rewritten as follows:

$$\sigma_{zz}'^{(G)} = c_{13}\varepsilon_r^{(G)} + c_{13}\varepsilon_\theta^{(G)} + c_{33}\varepsilon_z^{(G)}, \tag{6.3}$$

in which the strain components are obtained as follows:

$$\varepsilon_r^{(G)} = -\frac{\partial u_r^{(G)}}{\partial r},\ \varepsilon_\theta^{(G)} = -\frac{u_r^{(G)}}{r},\ \varepsilon_z^{(G)} = -\frac{\partial u_z^{(G)}}{\partial z},\ \varepsilon_{zr}^{(G)} = -\frac{1}{2}\left(\frac{\partial u_r^{(G)}}{\partial z} + \frac{\partial u_z^{(G)}}{\partial r}\right). \tag{6.4}$$

At this step, suppose that the unit circular uniform patch load is applied at $\Pi(z)$, then, one has the following relation:

$$\sigma_{zz}'^{(G)}(z,z_-) = c_{13}\varepsilon_r^{(G)}(z,z_-) + c_{13}\varepsilon_\theta^{(G)}(z,z_-) + c_{33}\varepsilon_z^{(G)}(z,z_-),$$

$$\sigma_{zz}'^{(G)}(z,z_+) = c_{13}\varepsilon_r^{(G)}(z,z_+) + c_{13}\varepsilon_\theta^{(G)}(z,z_+) + c_{33}\varepsilon_z^{(G)}(z,z_+). \tag{6.5}$$

By using above equation (6.5), one has the following:

$$\sigma_{zz}'^{(G)}(z,z_+) - \sigma_{zz}'^{(G)}(z,z_-) = c_{33}\left[\varepsilon_z^{(G)}(z,z_+) - \varepsilon_z^{(G)}(z,z_-)\right]. \tag{6.6}$$

Namely,

$$\varepsilon_z^{(G)}(z,z_+) - \varepsilon_z^{(G)}(z,z_-) = \frac{1}{c_{33}}\left[\sigma_{zz}'^{(G)}(z,z_+) - \sigma_{zz}'^{(G)}(z,z_-)\right] = \frac{1}{Ac_{33}}. \tag{6.7}$$

Since $\varepsilon_z^{(G)}(z,z_+) = \varepsilon_z^{(G)}(z_-,z)$ and $\varepsilon_z^{(G)}(z,z_-) = \varepsilon_z^{(G)}(z_+,z)$, the above equation (6.7) can thus be reduced to:

$$\varepsilon_z^{(G)}(z_+,z) - \varepsilon_z^{(G)}(z_-,z) = -\frac{1}{Ac_{33}}. \tag{6.8}$$